

1979

Prediction of fatigue strength of welded details, January 1979

Nicholas Zettlemyer

John W. Fisher

Follow this and additional works at: <http://preserve.lehigh.edu/engr-civil-environmental-fritz-lab-reports>

Recommended Citation

Zettlemyer, Nicholas and Fisher, John W., "Prediction of fatigue strength of welded details, January 1979" (1979). *Fritz Laboratory Reports*. Paper 463.
<http://preserve.lehigh.edu/engr-civil-environmental-fritz-lab-reports/463>

This Technical Report is brought to you for free and open access by the Civil and Environmental Engineering at Lehigh Preserve. It has been accepted for inclusion in Fritz Laboratory Reports by an authorized administrator of Lehigh Preserve. For more information, please contact preserve@lehigh.edu.

386-10(79)
**Lehigh
University**



High Cycle Fatigue of Welded Bridge Details

THE PREDICTION OF FATIGUE STRENGTH OF WELDED DETAILS

FRITZ ENGINEERING
LABORATORY LIBRARY

by

**Nicholas Zettlemyer
John W. Fisher**

**Fritz
Engineering
Laboratory**

Report No. 386-10 (79)

COMMONWEALTH OF PENNSYLVANIA

Department of Transportation

Bureau of Materials, Testing and Research

Leo D. Sandvig - Director
Wade L. Gramling - Research Engineer
Kenneth L. Heilman - Research Coordinator

Project 72-3: High Cycle Fatigue of
Welded Bridge Details

THE PREDICTION OF FATIGUE STRENGTH

OF WELDED DETAILS

by

Nicholas Zettlemyer

John W. Fisher

Prepared in cooperation with the Pennsylvania Department of Transportation and the U. S. Department of Transportation, Federal Highway Administration. The contents of this report reflect the views of the authors who are responsible for the facts and the accuracy of the data presented herein. The contents do not necessarily reflect the official views or policies of the Pennsylvania Department of Transportation, the U. S. Department of Transportation, Federal Highway Administration, or the Reinforced Concrete Research Council. This report does not constitute a standard, specification or regulation.

LEHIGH UNIVERSITY

Office of Research

Bethlehem, Pennsylvania

January 1979

Fritz Engineering Laboratory Report No. 386-10(79)

TABLE OF CONTENTS

	<u>Page</u>
ABSTRACT	iv
1. INTRODUCTION	1
1.1 Objectives and Scope	1
1.2 Fatigue Life Prediction	2
1.3 F_g Evaluation Approaches	5
1.4 Previous Work on the Stress Concentration/ Stress Intensity Relationship	7
2. STRESS CONCENTRATION EFFECTS	9
2.1 Crack Free Stress Analysis	9
2.1.1 Analytical Models	9
2.1.2 Stress Concentration Results	12
2.2 Stress Gradient Correction Factor	14
2.2.1 Green's Function	14
2.2.2 Typical Results	16
2.2.3 Prediction	16
3. STRESS INTENSITY	21
3.1 Other Correction Factors	21
3.1.1 Crack Shape Correction - F_e	21
3.1.2 Front Free Surface Correction - F_s	22
3.1.3 Back Free Surface Correction - F_w	23
3.2 Crack Shape Effects on F_g	27
3.3 Crack Shape Variations During Growth	27

	<u>Page</u>
3.4 Total Stress Intensity	29
3.4.1 Through Crack ($a/b = 0$)	30
3.4.2 Half-Circular Crack ($a/b = 1$)	35
3.4.3 Interpolation for Half-Elliptical Cracks ($0 < a/b < 1$)	38
3.4.4 F_s Variation at Typical Details	39
4. FATIGUE LIFE CORRELATIONS	41
4.1 Transverse Stiffeners Fillet-Welded to Flanges	43
4.2 Cover Plates with Transverse End Welds	46
5. SUMMARY AND CONCLUSIONS	49
6. TABLES	51
7. FIGURES	58
8. NOMENCLATURE	81
9. REFERENCES	85

ABSTRACT

This report provides a means of estimating the stress concentration effects when predicting the fatigue life of several welded details. The results of an analytical study of the fatigue behavior of welded stiffeners and cover plates were compared with the test data reported in NCHRP Reports 102 and 147. The comparison indicated that the variation in test data could be accounted for by considering the probable variation in initial crack sizes and crack growth rates.

The stress gradient correction factors developed for stiffeners and cover plates welded to beam flanges provide the necessary analytical tools for estimating the applicable stress intensity factors. In this study a lower bound crack shape relationship was utilized which was derived from cracks that formed at the weld toes of full size cover-plated beams.

1. INTRODUCTION

1.1 Objectives and Scope

It is well known that geometric stress concentration plays a significant role in fatigue crack growth at welded details. In fact, the categories of details established in the AASHTO Code⁽²⁾ primarily reflect differences in stress concentration conditions. Hence, in order to analytically predict the fatigue life of a detail, one must account for the local stress distribution as determined by the sudden change in geometry.

The primary objective of this report is the inclusion of stress concentration effects in the prediction of fatigue life. The coverage includes fillet-welded details of the stiffener and cover plate type. However, the basic techniques employed in the study could have been extended to any type of detail, even those which don't involve welding.

Besides stress concentration, fatigue life prediction also necessitates an understanding of the influence of crack shape on growth rates. A secondary objective of this report is clarification of the relationship between stress concentration and crack shape effects. Also, there is some investigation of crack shape variation during crack growth.

One implicit assumption made throughout the report is that the nominal stress range at the detail is known. Clearly, inclusion of

stress concentration in the analysis is of little use if the basic stress range is seriously in error.

1.2 Fatigue Life Prediction

Recent years have seen great strides in the development of techniques to analytically predict fatigue life. Fatigue crack growth per cycle, da/dN , can be empirically related to stress intensity factor, K , from linear fracture mechanics, as follows:⁽²⁷⁾

$$\frac{da}{dN} = C(\Delta K)^n \quad (1)$$

where ΔK is the range of stress intensity factor and C and n are based on material properties. By rearranging Eq. 1 and integrating between the initial and final crack sizes (a_i and a_f , respectively), the number of cycles, N , can be predicted as:

$$N = \frac{1}{C} \int_{a_i}^{a_f} \frac{1}{(\Delta K)^n} da \quad (2)$$

If the stress range is included in the expression, it takes on the following form:

$$N = \left[\frac{1}{C} \int_{a_i}^{a_f} \frac{1}{(\Delta K/S_r)^n} da \right] S_r^{-n} = AS_r^{-n} \quad (3)$$

Fisher experimentally found that parameter A changed value for different types of welded details. ⁽¹⁰⁾ The slope of the S_r -N curves, -n, is approximately constant at -3.0 for all categories. ^(10,11) C can be taken as constant for typical bridge steels (A36, A441, A514). ^(10,11) Initial crack size, a_i , is known approximately for some welded details ^(31,36) and a_f , being much larger than a_i , is usually of little consequence. Hence, fatigue life prediction for crack propagation rests primarily on the evaluation of the stress intensity factor range at the detail.

The range of stress intensity factor is often expressed as ΔK for a central through crack in an infinite plate under uniaxial stress, adjusted by numerous (superimposed) correction factors. ^(1,22,28,29,37)

$$\Delta K = CF * S_r \sqrt{\pi a} = F_s F_w F_e F_g * S_r \sqrt{\pi a} \quad (4)$$

CF is the combined correction factor as a function of crack length-plate width ratio a/w , crack shape ratio a/b , and geometry. F_s is the correction associated with a free surface at the crack origin (the front free surface), F_w accounts for a free surface at some finite length of crack growth (also called the back surface or finite width correction),

and F_e adjusts for shape of crack front (often assumed to be elliptic with major semidiameter b and minor semidiameter a). While in fracture problems stress intensity often includes a plastic zone correction factor, F_p , it is usually disregarded in fatigue analyses since small stress ranges and reversed yielding cause the crack tip plastic zone to be small. (22,23,30,37)

F_g is the factor which accounts for either a nonuniform applied stress (such as bending) or a stress concentration caused by the detail geometry. This stress gradient should not be confused with that which always occurs at the crack tip. F_g corrects for a more global condition than exists at the crack tip. Yet, for stress concentration situations F_g corrects for a more local condition than the nominal stress (strength of materials type) at the detail. Whether the applied stress is non-uniform or a stress concentration exists, S_r represents an arbitrarily selected stress range (usually the nominal maximum value at the detail). Therefore, F_g is inseparably linked to the choice of S_r .

Values of the various correction factors are dependent on the specific overall geometry, crack shape, and distribution of applied stress. Solutions for CF of many idealized problems are available. (23,32,34,35) However, practical bridge details present distinct analytical difficulties - particularly in evaluating F_g . Cracks normally emanate from weld toes^(9,10) near which varying degrees of stress concentration exist. For some geometries the crack quickly grows out of this concentration region; for other geometries the effect of concentration

is sustained over a broad range of crack sizes. Fillet-welded connections have the added difficulty that they present a theoretically singular stress condition (neglecting yielding) right at the weld toe. Therefore, F_g has been impossible to obtain in a closed-form fashion. Numerical techniques such as the finite element method normally must be employed.

1.3 F_g Evaluation Approaches

Based on Eq. 2 life prediction involves summing the cycle lives for increments of crack growth. F_g as well as other correction factors must be known for each increment. Three approaches are available for determining F_g for varying crack size; all approaches involve finite element analyses. The first, normally termed a compliance analysis, necessitates analyzing the detail for different lengths of embedded crack. The strain energy release rate, \mathcal{U} , is found as a function of the slope of the compliance-crack length curve.⁽¹⁸⁾ Irwin showed that there is a direct relationship between \mathcal{U} and the stress intensity factor.^(19,20) Thus, K can be found and compared, if desired, with some base K for a specimen lacking the influence of a stress gradient (i.e., $F_g = 1.0$). The ratio of the two stress intensity factors yields F_g for the actual detail under investigation.

A second relatively new approach incorporates special elements with inverse singularity for modeling of the crack tip. These elements permit accurate resolution of the displacements and stresses in the

crack tip region. Both displacement and stress are directly related to stress intensity and, as before, F_g is found by dividing by some base K . Once again, a separate analysis is required for each crack depth.

Both of the above methods can be very expensive and require extensive time. A compliance analysis also presents accuracy difficulties at very small and very large crack depths. A more reasonable alternative exists which requires only one stress analysis for a given detail geometry. Bueckner and Hayes showed that \mathcal{U} can be found from the stresses in the crack free body which act on the plane where the crack is to later exist. (8,16). Irwin implied this when he found \mathcal{U} by considering the energy needed to reclose a crack. (19) Based on this concept (often called superposition or difference state) it is possible to describe known stress intensity solutions for stresses or concentrated loads applied directly to crack surfaces as Green's functions for loading remote from the crack. (28,34,35) The stress or concentrated load is simply adjusted to suit the stress distribution along that plane with the crack absent. (A concentrated load is represented by stress applied to an incremental area. Through integration, numerical or closed-form, any stress distribution can be represented.) Depending on which Green's function is used, F_g alone or a combination of correction factors can be evaluated. The only requirement is that the crack path be known. Since actual tests have provided information on crack paths, (7,9,10,12) method three is employed in the study.

1.4 Previous Work on the Stress Concentration/Stress Intensity Relationship

Accurate analysis of the influence of stress concentration on stress intensity stems from Bowie's work on cracks emanating from circular holes. (6) Since then good estimates of K have been determined for cracks growing from elliptical holes, rectangular cutouts, and all sorts of notches. (24,26,32,34) With regard to fillet-welded connections, Frank's work on cruciform joints marks an early intensive effort to develop an expression for F_g . (12) A similar study was pursued by Hayes and Maddox shortly thereafter. (15) Unfortunately, the numerical conclusions of these two investigations weren't in agreement. Further, the accuracy of each was questionable at very small crack sizes. Gurney later tried to resolve the differences and did succeed in producing several helpful graphs involving the geometric variables. (14) However, no general formulas were developed and the accuracy at very small crack sizes was not known. Moreover, there was no assurance that graphs or expressions developed by any of the three studies could be applied to other, more complex, fillet-welded bridge details.

The analytical approach used to find F_g in Refs. 12, 14, and 15 was that of a compliance analysis based on finite element discretization of the joint. The Green's function technique was early used by Kobayashi, (21) who successfully estimated Bowie's results, and others. (28,35) Later, Albrecht developed an approach to F_g for fillet-welded joints using a Green's function. (1) However, no parametric study was conducted.

Use of finite elements with inverse singularity to analyze welded details has not yet appeared in the literature although this approach has promise for the future. One current need is the development of three-dimensional elements with the singularity condition.

2. STRESS CONCENTRATION EFFECTS

2.1 Crack Free Stress Analysis

2.1.1 Analytical Models

The overall detail geometries for the stiffener and cover plate investigations are shown in Figs. 1 and 2, respectively. In both cases the detail was assumed to exist on both sides of the beam web which, therefore, marks a plane of symmetry. Uniform stress was input to the details at a position far enough removed from the fillet weld so as to exceed the limit of stress concentration effects. In both details the flange width was held constant. The fillet weld angle was set at 45 degrees.

The thickness of a stiffener is generally small compared to the flange thickness, T_f . Hence, the stiffener itself was omitted from Fig. 1. The variable under investigation was the weld leg, Z . Z can be expected to range between $0.25 T_f$ and $1.00 T_f$. The three values of Z selected for this study were $0.32 T_f$, $0.64 T_f$, and $0.96 T_f$. A stress concentration analysis was completed for each value.

A pilot study on the cover-plated detail (Fig. 2) revealed that stress concentration reaches a plateau with increasing attachment length. Hence, the length of cover plate was set so as to

ensure maximum concentration conditions. The width of cover plate was held constant and the weld size was assumed constant along the cover plate edge. The variables studied were the weld leg, Z , and cover plate thickness, T_{cp} . The weld leg sizes considered were the same as for the stiffener detail and the cover plate thickness was taken as $0.64 T_f$, $1.44 T_f$, and $2.0 T_f$.

Both of the details were initially analyzed three-dimensionally. However, in order to reduce costs this first level of investigation was only of sufficient accuracy to provide reasonable input to a more local, two-dimensional stress analysis. For the two details studied, fatigue cracks normally originate along the weld toe and propagate through the flange thickness.^(9,10) Hence, the plane of interest for two-dimensional stress analysis was the section shown in Figs. 1 and 2. Pilot studies showed that the stress concentration increases slightly as the section gets nearer the web line. Therefore, the specific section for two-dimensional analysis was taken right at the web line.

An existing finite element computer program, SAP IV,⁽⁴⁾ was used for the entire stress analysis effort. The program is intended for elastic analysis only; Young's modulus was set at 29,600 ksi and Poisson's ratio was taken to be 0.30. A three-dimensional coarse mesh, using brick elements, was established for each detail and subjected to uniform stress. Nodal displacement output from the 3D mesh was then input to a two-dimensional fine mesh. Nodal

displacement output from the fine mesh was subsequently input to an ultra fine mesh which was very local to the weld toe. Finally, the element stress concentrations were extrapolated to give a maximum stress concentration factor, SCF, right at the weld toe.

Figures 3 and 4 show the coarse meshes used for each detail. The dashed lines are intended to indicate how the variable cover plate thickness and/or weld leg dimension were effected. In all cases the flange discretization and actual thickness (0.78 in.) were held constant. Also, the first line of weld elements adjacent to the overall weld toe had constant size. For both models, displacements perpendicular to lines of symmetry were prevented. Displacement perpendicular to each plan view was prevented along the web line and, in the stiffener case, also along the weld line of symmetry (to simulate the stiffener).

Figures 5 and 6 show the fine and ultra fine meshes which were common to both detail investigations. Planar elements of constant thickness were used throughout. The heavy lines denote the outline of previous mesh elements. Displacements at common mesh nodes along the border were known from the prior analysis; displacements at newly created nodes at the boundary were found by linear interpolation between known values.

The need for an ultra fine mesh deserves further explanation. The assumed geometry at the weld toe creates an elastic stress

singularity condition. Hence, a decrease in mesh size adjacent to the toe yields ever higher stress values. However, the stresses somewhat removed from the toe become stabilized and the distance to stabilization decreases with decreasing mesh size. Since the analyst is interested in accuracy of stresses beyond the initial crack size, it seemed reasonable to ensure the mesh size was at least as small as the initial crack size. For the assumed flange thickness (0.78 in.), the minimum mesh size was 0.001 in. Several investigations have established this as a lower limit of initial crack size. (31,36)

A hypothetical maximum stress concentration factor was obtained by fitting a fourth order polynomial through the averaged concentration values on either side of the node line down from the weld toe in the ultra fine mesh.

2.1.2 Stress Concentration Results

The SCF values for each stiffener and cover plate geometry analyzed are plotted in Fig. 7. SCF increases for increasing stiffener weld size, but decreases for increasing cover plate weld size. These trends are similar to Gurney's findings for non-load-carrying and load-carrying cruciform joints. (14) Apparently, a transition from a non-load-carrying to load-carrying condition occurs as the attachment length along the beam increases.

Regression analyses for the stiffener and cover plate data suggest the following equations: (38)

Stiffeners:

$$SCF = 1.621 \log \left(\frac{Z}{T_f} \right) + 3.963 \quad (5)$$

Cover Plates:

$$SCF = -3.539 \log \left(\frac{Z}{T_f} \right) + 1.981 \log \left(\frac{T_{CP}}{T_f} \right) + 5.798 \quad (6)$$

The standard errors of estimate, s , for Eqs. 5 and 6 are 0.0019 and 0.0922, respectively.

Stress concentration factor decay curves for sample stiffener and cover plate details are plotted in Fig. 8. Each K_t curve eventually drops below 1.0 due to the equilibrium requirements. The cover plate is seen to cause much more disruption to stress flow than does the stiffener. In both cases the stress concentration is most pronounced at small crack sizes. Unfortunately, most of the fatigue life is expended in the same range. (9)

2.2 Stress Gradient Correction Factor

2.2.1 Green's Function

The Green's function or superposition approach makes use of stress intensity solutions for loading directly on the crack surface. Use of the Green's function suggested by Albrecht and Yamada leads to the following stress intensity expression:⁽¹⁾

$$K = \sigma \sqrt{\pi a} * \frac{2}{\pi} \int_0^a \frac{K_t}{\sqrt{a^2 - \ell^2}} d\ell \quad (7)$$

where σ is the nominal stress on the section and K_t is the crack free stress concentration factor at position ℓ . Since $\sigma \sqrt{\pi a}$ is the stress intensity for a through crack under uniform stress, the stress gradient correction factor, F_g , at crack length a is:

$$F_g = \frac{2}{\pi} \int_0^a \frac{K_t}{\sqrt{a^2 - \ell^2}} d\ell \quad (8)$$

If crack length, a , and distance, ℓ , are both nondimensionalized by the flange thickness, T_f , Eq. 8 becomes:

$$F_g = \frac{2}{\pi} \int_0^\alpha \frac{K_t}{\sqrt{\alpha^2 - \lambda^2}} d\lambda \quad (9)$$

where $\alpha = a/T_f$

$\lambda = \ell/T_f$.

Occasionally it is possible to express K_t by a polynomial equation such as:

$$\frac{K_t}{SCF} = 1 + A\lambda + B\lambda^2 + C\lambda^3 + D\lambda^4 \quad (10)$$

where A, B, C, and D are dimensionless constants. For such a representation of stress concentration, Eq. 9 can be solved in a closed-form manner. (37,38)

$$\frac{F_g}{SCF} = 1 + \frac{2A}{\pi} \alpha + \frac{B}{2} \alpha^2 + \frac{4C}{3\pi} \alpha^3 + \frac{3D}{8} \alpha^4 \quad (11)$$

Equation 11 can be applied to polynomials of lesser order by merely equating the appropriate decay constants to zero.

It is difficult to make use of Eq. 11 for stiffeners and cover plates since the typical concentration curves (Fig. 8) are not well suited to polynomial representation. Hence, Eq. 8 usually can't be solved in a closed-form manner. However, a numerical solution is easily devised as suggested by Albrecht. (1)

$$F_g = \frac{2}{\pi} \sum_{j=1}^m K_{tj} \left[\arcsin \left(\frac{\ell_{j+1}}{a} \right) - \arcsin \left(\frac{\ell_j}{a} \right) \right] \quad (12)$$

in which K_{tj} is the stress concentration factor in element j of the finite element discretization or the average of two adjacent elements, both of equal distance along opposite sides of the crack path. Limit m is the number of elements to crack length a .

2.2.2 Typical Results

Figure 9 shows the predicted trend of the stress gradient correction in relation to stress concentration at typical welded details. Both the F_g and K_t curves begin at SCF. Each decays to a level below 1.0 although the F_g decay is less rapid. In general, the separation of the two curves at any point other than the origin depends on detail geometry.

Figure 10 presents F_g decay curves (F_g/SCF) for sample stiffener and cover plate details. Usually, the curves for cover plates are below those for stiffeners since the SCF values are higher. It is also apparent that details with similar SCF often have different decay rates. This fact means that the F_g curve is related to a different mix of geometrical parameters than is SCF.

2.2.3 Prediction

It is highly advantageous to have a means of obtaining F_g for different details without individual finite element studies. One approximate method is to represent the F_g equation as:

$$\frac{F_g}{SCF} = \frac{1}{1 + \frac{1}{d} \alpha^q} \quad (13)$$

For a typical stiffener geometry, Table 1 shows constants d and q can be taken as 0.3602 and 0.2487, respectively. An average cover plate detail is reasonably represented by values of 0.1473 and 0.4348.

A second, more precise method of obtaining F_g is also available. It can be seen that the characteristics of the F_g curve (Fig. 9) are quite similar to features of stress concentration decay (based on gross section stress) from the end of an elliptical hole in an infinite, uniaxially stressed plate.^(5,25) Each curve begins at the maximum concentration factor, SCF, and decays to a value near one. (The asymptote for the elliptical hole is exactly 1.) Therefore, it is possible to correlate a hypothetical hole to actual F_g curves (Fig. 10) such that any F_g curve can be estimated from the appropriate hole shape and size.

The elliptical hole shape determines the maximum stress concentration factor.

$$SCF = 1 + 2 \frac{g}{h} \quad (14)$$

in which g and h are the hole major and minor semidiameters, respectively. Conversely, given the maximum concentration at a detail (Eqs. 5 and 6), the correlated hole shape can be determined.

Figure 11 shows the stress concentration factor decay from an elliptical hole is dependent on both the hole shape and its absolute size. A smaller hole has a more rapid concentration decay. In order to predict F_g from the elliptical hole K_t curve, it is necessary to establish the proper ellipse size - semidiameter g. Such correlation is here based on equal life prediction for crack growth through the flange thickness.

Stress concentration decay along the major axis of an elliptical hole (uniaxial tension in minor axis direction) can be expressed as: (5)

$$K_t = \left[\frac{1}{8} \left\{ 1 - 2e^{2\gamma} + e^{4\gamma} \right\} \left\{ 3 - 4e^{-2\eta} + e^{-4\eta} \right\} - \frac{1}{8} e^{4(\gamma-\eta)} \right. \\ \left. + \sinh(2\eta) \left\{ \cosh(2\eta) + \frac{1}{3} \cosh(2\gamma) - \frac{3}{2} \right\} \right] / \left(\cosh(2\eta) - 1 \right)^2 \quad (15)$$

in which η is the general elliptic coordinate and γ is the specific value of η associated with the hole perimeter. The elliptic coordinate can readily be evaluated.

$$\cosh(\gamma) = \left[\frac{1}{1 - \frac{h}{g}^2} \right]^{1/2} \quad (16)$$

$$\cosh(\eta) = \left\{ 1 + \frac{a}{g} \right\} \cosh(\gamma) \quad (17)$$

For any given geometry and assumed value of crack length, a , the stress concentration factor, K_t , is known if g is known. Further, if g has been correlated to equate K_t and F_g , then the stress gradient correction factor is also established.

A correlation study for the geometries investigated related the optimum ellipse size to the various geometrical parameters and initial crack size, a_i . The regression curves which resulted are: (38)

Stiffeners:

$$\begin{aligned} \frac{g}{T_f} = & -0.002755 + 0.1103 \left(\frac{Z}{T_f} \right) - 0.02580 \left(\frac{Z}{T_f} \right)^2 \\ & + 0.6305 \left(\frac{a_i}{T_f} \right) - 7.165 \left(\frac{a_i}{T_f} \right)^2 \end{aligned} \quad (18)$$

Cover Plates:

$$\begin{aligned} \frac{g}{T_f} = & 0.2679 + 0.07530 \left(\frac{Z}{T_f} \right) - 0.08013 \left(\frac{Z}{T_f} \right)^2 \\ & + 0.2002 \log \left(\frac{T_{cp}}{T_f} \right) + 1.391 \left(\frac{a_i}{T_f} \right) - 11.74 \left(\frac{a_i}{T_f} \right)^2 \end{aligned} \quad (19)$$

The standard errors of estimates, s , for Eqs. 15 and 16 are 0.0041 and 0.0055, respectively.

Figure 12 compares the K_t curve at a sample cover plate detail with the actual F_g curve from the Green's function (Eq. 12) and the F_g curve from the correlated ellipse. It is apparent the two F_g curves are in close agreement and cross over each other twice. Such is also common for stiffener details.

3. STRESS INTENSITY

3.1 Other Correction Factors

3.1.1 Crack Shape Correction - F_e

F_e is based upon Green and Sneddon's solution for the opening displacement of an embedded elliptical crack under perpendicular stress. (13) Irwin (29) made use of Westergaard's relationship between crack opening displacement and stress intensity. The resulting F_e for any position along the crack front, described by angle ϕ to the major axis, is:

$$F_e = \frac{1}{E(k)} \left[1 - k^2 \cos^2 \phi \right]^{1/4} \quad (20)$$

where k is 1.0 minus the ratio a/b squared and $E(k)$ is the complete elliptic integral of the second kind. Interest is usually directed to the minor axis end of the ellipse where $\phi = \pi/2$. For this particular position:

$$F_e = \frac{1}{E(k)} \quad (21)$$

Equation 20 was derived on the basis of uniform tension across the crack surface. While it may be argued that variable tension will modify the result, such is taken into account by the F_g correction later described. Hence, F_e is maintained in its original form for stress intensity estimates.

3.1.2 Front Free Surface Correction - F_s

F_s is generally necessary for edge cracks since stress, not displacement, is zero on the free boundary. A girder web as well as attachments like stiffeners and cover plates can provide some restriction to displacement at weld toes or terminations. The magnitude of such restriction is not known to any specific degree although it is estimated to be modest. Furthermore, inclusion of an F_s other than 1.0 usually leads to a lower bound or conservative fatigue life estimate. Hence, front free surface displacement restriction by attachments is disregarded in this report.

Tada and Irwin have tabulated the variability of F_s with the distribution of stress applied to the crack. ^(34,35) Table 2 shows this variability for the types of crack shapes and stress distributions of interest at welded stiffener and cover plate details. If a through crack exists and the stress is uniform over the crack length, F_s is 1.122. If the stress varies linearly to zero at the crack tip, F_s is 1.210. And if a concentrated load exists at the

crack origin, F_s is 1.300. Obviously, if the stress distribution decreases from the crack origin more rapidly than the linear condition, F_s must have a value between 1.210 and 1.300.

Reference 35 also directs attention to the half-circular crack. For a uniform stress over the entire crack plan area, F_s at the crack tip is 1.025. For a stress which varies linearly to zero at the crack tip, F_s at the same location is 1.085. The solution for a concentrated load at the crack origin is not known. F_s for this condition is estimated at 1.145, which incorporates twice the increment increase exhibited by changing from a uniform to a linear stress pattern.

3.1.3 Back Free Surface Correction - F_w

The solutions for F_s consider infinite half spaces. When the space is not infinite, thought must be given to the back surface correction, F_w . Once again the form of the correction depends on stress distribution and crack shape. However, F_w also is quite sensitive to whether or not the section is permitted to bend as crack growth occurs. The bending tendency is natural for any strip in which crack growth is not symmetrical with respect to the strip centerline.

The literature often cites two forms of F_w (almost interchangeably) for the symmetrical crack cases presented in Fig. 13. (28,32,34,35) These two expressions are also applicable to nonsymmetrical crack configurations where bending is prevented by imposed boundary conditions. Hence, the strips in Fig. 14 are comparable to those in Fig. 13. At real structural details the roller supports might be provided by a web, stiffener, and/or cover plate.

Bending amplifies the back surface correction - particularly at high values of a/w where more bending occurs. If the rollers on either strip of Fig. 14 are removed, the back surface correction takes on the following form: (34,35)

$$F_w = Q^* \left[\frac{2}{\pi\alpha} \tan \left(\frac{\pi\alpha}{2} \right) \right]^{1/2} \quad (22)$$

where
$$Q = \frac{0.752 + 2.02\alpha + 0.37 \left[1 - \sin \left(\frac{\pi\alpha}{2} \right) \right]^3}{1.122 \cos \left(\frac{\pi\alpha}{2} \right)}$$

$$\alpha = \frac{a}{w}$$

The coefficient, Q , by which the tangent correction is modified is plotted in Fig. 15.

Table 3 gives the back surface corrections for through cracks with and without bending permitted. Without bending the familiar secant correction is used for a uniform stress while the secant is amplified as stress concentration occurs at the crack origin. This amplification has maximum value $1.297 \sqrt{\pi/2}$ for a concentrated load at the crack origin and $\alpha = 1.0$. Both no bending solutions stem from a finite width plate with a central through crack.⁽³⁴⁾ A linearly varying stress case is assumed to be the average of the two extremes. A sharper stress decay has a correction somewhere between the concentrated load and the linearly varying stress values.

The back surface corrections associated with bending show significant amplification of the secant correction. Since the tangent and secant corrections are similar, Fig. 15 gives a good indication of the amplification for both cases when uniform stress is applied. The amplification factor for a concentrated load is much higher than that for a uniform stress. For example, at $\alpha = 0.6$ the uniform stress amplification is 1.97 while the concentrated load amplification is 6.07 (Table 2). These back surfaces solutions are directly linked to front surface corrections since bending demands lack of symmetry. The combined correction factors for through cracks found in Refs. 34 and 34 were divided by the associated front surface corrections (Table 1) to isolate the back surface correction factors.

The choice between bending and no bending depends on the structural detail as well as how the crack is growing. Fatigue crack growth at welded stiffeners, cover plates, and other common girder attachments is rarely symmetrical. Yet, bending is usually limited by virtue of the girder web and/or the attachment itself.⁽⁷⁾ Hence, the no bending corrections are considered to be most applicable in typical bridge structures.

To this point all discussion of back free surface correction factors has centered on the through crack configuration ($a/b = 0$). Maddox⁽²³⁾ recently condensed the work of numerous researchers and estimated how F_w varies for crack shape ratios and α values between zero and 1.0. Uniform stress and unrestricted bending were assumed. His results essentially agree with Table 2 when a/b equals zero, but vary nonlinearly to almost 1.0 for any α value when a/b equals 1.0. In other words, F_w might well be disregarded for the half-circular crack. The net ligament on either side of the crack inhibits bending and significantly limits the crack from sensing the upcoming free surface.

The curves Maddox produced are approximations since few data points exist for crack shape ratios between zero and 1.0. Nevertheless, it is reasonable to assign F_w a value of 1.0 for any α if the crack shape is circular, regardless of the bending and stress distribution considerations. The fact that some references show an F_w value slightly above 1.0 when α is large and $a/b = 1.0$ is not important since most fatigue life is expended at small α .

3.2 Crack Shape Effects on F_g

The entire development of Chapter 2 was based upon a through crack configuration ($a/b = 0$). Implementation of each of the analytical approaches to F_g usually involves this assumption although solutions for other crack shapes are actually possible. Moreover, it is worthwhile noting F_g varies with crack shape and such variance should be taken into account in the fatigue life prediction process.

Table 4 has been developed using through and circular crack Green's functions for a crack in infinite solid.^(1,35) The table shows that the values for F_g diverge as the stress decay becomes more rapid. The limiting ratio, Y , for a concentrated load at the crack origin is estimated to be 0.548. This number represents twice the deviation from 1.0 recorded between the uniform and linear stress cases.

3.3 Crack Shape Variations During Growth

A major factor affecting correction factors is the crack shape during growth. Gurney has found that the importance increases as the stress concentration or detail severity increases.⁽¹⁴⁾ Normally, cracks are idealized as elliptical although experimenters have recognized that most cracks are actually irregular in shape.^(29,33)

Crack shape ratio, a/b , is dependent upon several variables. One of them is the proximity of free surfaces, as distinguished by the ratio

a/w. Another is the overall geometry of the detail which affects F_g and, in turn, a/b. Therefore, plates of different width (or thickness if crack is growing in that direction) can cause different crack shapes to occur. (37)

Also, study has shown that cracks begin at several sites along a transverse weld toe, but eventually they coalesce. (10,37) Coalescence occurs several times during the growth process.

In order to establish a crack shape relationship it is necessary to rely on actual measurements of crack size during growth. These measurements can only be performed accurately by breaking apart structural details at different crack growth stages. Reference 37 has reviewed and compared the available crack shape variation equations for growth at the toe of a transverse fillet weld. References 10 and 23 provide equations relating single crack shape to crack depth that are in marked disagreement with each other. The relationship suggested in Ref. 23 provides a lower bound (conservative) characterization of early crack shapes. This equation is:

$$b = 0.132 + 1.29 a \quad (23)$$

where a = crack depth and ellipse minor semidiameter (in.)

b = half surface length of crack and ellipse major semidiameter (in.)

The relationship suggested in Ref. 10

$$b = 1.088 a^{0.946} \quad (24)$$

was observed to provide an upper bound relationship.

When coalescence begins Eq. 23 or 24 no longer applies since the shape trend is toward flatter rather than more circular cracks. The multiple crack data in Ref. 10 suggested the following crack shape relationship:

$$b = 3.284 a^{1.241} \quad (25)$$

However, an examination of cracks at the weld toes of full size cover-plated beams suggested that a lower bound for the crack shape during the coalescence phase was provided by the relationship. (39)

$$b = 5.462 a^{1.133} \quad (26)$$

All four of the crack shape relationships are plotted in Fig. 16 and compared with the data for full scale cover-plated beam details. The intersection of Eqs. 23 and 26 is near a crack depth of 0.055 in. These two equations are employed for use at all transverse welds, regardless of detail geometry, pending further studies.

3.4 Total Stress Intensity

Fatigue life analysis of typical welded details involves estimating the stress intensity for a nonuniform stress distribution. Figure 17 shows the type of distribution which is common to any stress concentration region. This distribution may be separated into uniform and variable constituents. Since stress intensity is linear in stress, σ , superposition applies provided the crack displacement mode is unchanged. (34,35) Hence, the total

stress intensity can be found by adding the stress intensities, K_u and K_v , for two "sub" stress distributions which sum to the total stress distribution. The stress intensity correction factors for the uniform stress distribution are known while the correction factors applicable to the variable subdistribution can be estimated. (37)

Consideration must also be given to crack shape effects on stress intensity. Thus, an approximate procedure is adopted whereby the total stress intensity defined above is established for the extremes of crack shape ($a/b = 0$ and $a/b = 1$). A linear interpolation between these limits approximates the stress intensity for the actual crack shape at any crack depth. Obviously, a very important input to stress intensity estimates is the crack shape variation.

3.4.1 Through Crack ($a/b = 0$)

Using the correction factors of Art. 3.1 (no bending) the stress intensity for uniform stress can be written as:

$$K_u = 1.122 * K_{t\alpha} * \sigma \sqrt{\pi\alpha} * \left[\sec\left(\frac{\pi\alpha}{2}\right) \right]^{1/2} \quad (27)$$

where $\alpha = a/T_f$

T_f = flange thickness

$K_{t\alpha}$ = stress concentration factor at position

Since this is a through crack, F_e is 1.0. It is apparent that for uniform stress the stress gradient correction has constant value $K_{t\alpha}$.

Development of the stress intensity for varying stress is more complex. Table 2 shows that F_s is between 1.300 and 1.210. The correct intermediate value depends on the shape of the actual stress concentration factor decay curve (K_t) relative to a linear decay line. Figure 18a demonstrates that the proximity to a linear condition varies with α . As α increases, F_s increases from 1.210 to a value near 1.300.

If F_{s1} represents the desired value of F_s , then:

$$F_{s1} = 1.300 - \psi (1.300 - 1.210) = 1.300 - 0.09 \psi \quad (28)$$

where ψ = measure of proximity to linearity; has value 1.0 if actually linear.

ψ can be evaluated on the basis of Fig. 18b. ξ represents that value of λ at which the slope of the stress concentration decay curve equals the slope of a hypothetical straight decay line from SCF to α . The lower limit of ξ is zero while the upper limit is $\alpha/2$. Thus, ψ is taken as:

$$\psi = \frac{\xi}{\alpha/2} = \frac{2\xi}{\alpha} \quad (29)$$

Proper resolution of Eq. 29 depends on knowledge of the concentration factor decay curve which varies for each detail geometry. However, since the change in F_{s1} is usually small over the full

range of ψ values, reasonable accuracy is attained by using an approximate equation of the following form for all cases:

$$\frac{K_{t\lambda}}{SCF} = \frac{1}{1 + \frac{1}{c} \lambda^p} \quad (30)$$

where $\lambda = \ell/T_f$

ℓ = position in the crack growth direction

c, p = constants.

If the stress gradient results for average stiffener and cover plate geometries are used, the values of c and p summarized in Table 1 result.

Equation 30 can be used to evaluate the indicated slopes at $\lambda = \alpha$ and $\lambda = \xi$. A nonlinear "characteristic" equation results which must be solved for ξ .

$$\frac{1}{c^2} \xi^{2p} + \frac{2}{c} \xi^p - \frac{p}{D} \xi^{p-1} + 1 = 0 \quad (31)$$

where $D = \frac{\alpha^{p-1}}{1 + \frac{1}{c} \alpha^p}$

The solution of Eq. 31 is readily obtained for any given α by the bisection method. Thus, ψ can be calculated and F_{s1} defined.

ψ is also employed in calculating the appropriate back free surface correction, F_w , for the variable stress subdistribution. From Art. 3.1.3 the expression for F_w can be developed in a manner similar to F_{s1} .

$$F_w = C * \left[\sec\left(\frac{\pi\alpha}{2}\right) \right]^{1/2} \quad (32)$$

where $C = \left(1 - \frac{\psi}{2}\right) \left[1.297 - 0.297 \cos\left(\frac{\pi\alpha}{2}\right) \right] \left[\frac{\pi\alpha}{2} \operatorname{cosec}\left(\frac{\pi\alpha}{2}\right) \right]^{1/2} + \frac{\psi}{2}$

The stress gradient correction factor for the subdistribution, \bar{F}_g , is related to F_g calculated for the whole distribution. Albrecht's Green's function (Eq. 7) in nondimensional form yields:

$$K = \sqrt{\pi a} * \frac{2}{\pi} \int_0^\alpha \frac{\sigma_\lambda}{\sqrt{\alpha^2 - \lambda^2}} d\lambda \quad (33)$$

where $\sigma_\lambda = \sigma(K_{t\lambda} - K_{t\alpha})$ for the subdistribution.

Hence,
$$\bar{F}_g = \frac{2}{\pi} \int_0^\alpha \frac{(K_{t\lambda} - K_{t\alpha})}{\sqrt{\alpha^2 - \lambda^2}} d\lambda \quad (34)$$

Equation 9 yields the following relationship:

$$\bar{F}_g = F_g - K_{t\alpha} \quad (35)$$

The stress intensity expression for the variable stress subdistribution can now be estimated using Eqs. 28, 32 and 35.

$$K_v = F_{s1} * (F_g - K_{t\alpha}) * \sigma \sqrt{\pi a} * C \left[\sec\left(\frac{\pi\alpha}{2}\right) \right]^{1/2} \quad (36)$$

Combining Eqs. 27 and 36 results in the total stress intensity expression for stiffeners and cover plates with through cracks.

$$K = \left\{ 1.122 * K_{t\alpha} * \left[\sec\left(\frac{\pi\alpha}{2}\right) \right]^{1/2} + F_{s1} * (F_g - K_{t\alpha}) * C \left[\sec\left(\frac{\pi\alpha}{2}\right) \right]^{1/2} \right\} * \sigma \sqrt{\pi a} \quad (37)$$

It is helpful to rearrange Eq. 37 in the following form:

$$K = [F_{s1} * C + (1.122 - F_{s1} * C) * X] * F_g * \sigma \sqrt{\pi a} * \left[\sec\left(\frac{\pi\alpha}{2}\right) \right]^{1/2} \quad (38)$$

where $X = \frac{K_{t\alpha}}{F_g}$

Evaluation of X in Eq. 38 can be performed with the stress gradient correction provided by the artificial ellipse correlation given in Art. 2.2.3. It is also possible to use the approximate equation for F_g which sacrifices little accuracy.

$$\frac{F_g \alpha}{SCF} = \frac{1}{1 + \frac{1}{d} \alpha^q} \quad (39)$$

For average stiffener and cover plate geometries, d and q are given in Table 1. By combining Eqs. 30 and 39, X becomes:

$$X = \frac{1 + \frac{1}{d} \alpha^q}{1 + \frac{1}{c} \alpha^p} \quad (40)$$

3.4.2 Half-Circular Crack (a/b = 1)

The stress intensity for the uniform stress subdistribution on a half-circular crack can be defined as: (35)

$$K_u = 1.025 * K_{t\alpha} * \frac{2}{\pi} * \sigma \sqrt{\pi a} \quad (41)$$

Crack shape correction, F_e , is represented by $2/\pi$ and F_w is assumed to be 1.0.

For the varying stress condition F_s is represented by F_{s2} :

$$F_{s2} = 1.145 - 0.06 * \psi \quad (42)$$

ψ is the same value calculated for the through crack case.

The stress gradient correction associated with the circular crack front, \bar{F}'_g , is defined:

$$\bar{F}'_g = F'_g - K_{t\alpha} \quad (43)$$

Article 3.2 recognized that F'_g is not of the same numerical value as F_g calculated for the through crack Green's function unless the applied stress has uniform distribution.

Equations 42 and 43 can be used to develop the stress intensity factor for the variable stress subdistribution.

$$K_v = F_{s2} * (F'_g - K_{t\alpha}) * \frac{2}{\pi} * \sigma \sqrt{\pi a} \quad (44)$$

Adding K_v to K_u (Eq. 41) gives the total K for the half-circular crack shape.

$$K = \left[1.025 * K_{t\alpha} * \frac{2}{\pi} + F_{s2} * (F'_g - K_{t\alpha}) * \frac{2}{\pi} \right] * \sigma \sqrt{\pi a} \quad (45)$$

Rearranging Eq. 45 gives:

$$K = \left[F_{s2} * Y + (1.025 - F_{s2}) * X \right] * F_{g\alpha} * \frac{2}{\pi} * \sigma \sqrt{\pi a} \quad (46)$$

where $Y = \frac{F'_g}{F_g}$

Evaluation of ratio Y is assisted by Table 4. However, it must be borne in mind that F_g and F'_g are evaluated for the total stress distribution, not just the variable subdistribution. The Y ratio for the total distribution is dependent on the relative influence of the variable stress subdistribution as compared with the uniform stress distribution. Hence, Y is taken as the sum of two parts.

$$Y = W * Y' + (1-W) * Y'' \quad (47)$$

where $Y' = 0.548 + 0.226 * \psi$

$$Y'' = 1.000$$

W = weighting factor of variable stress subdistribution relative to the uniform stress subdistribution.

Factor W may be based upon the ratio of the two shaded areas under the concentration decay curve in Fig. 19.

$$W = \frac{A_v}{A_u} = \frac{\int_0^\alpha (K_{t\lambda} - K_{t\alpha}) d\lambda}{K_{t\alpha} * \alpha} = \frac{\int_0^\alpha K_{t\lambda} d\lambda}{K_{t\alpha} * \alpha} - 1 \quad (48)$$

Substituting Eq. (5) into (23) gives:

$$W = \frac{\int_0^{\alpha} \frac{1}{1 + \frac{1}{c} \lambda^p} d\lambda}{\frac{\alpha}{1 + \frac{1}{c} \alpha^p}} - 1 \quad (49)$$

The integral in the numerator can be evaluated numerically; therefore, factor W is easily obtained. However, W decreases with increasing relative crack length and must be reevaluated for each crack position.

For the benefit of later calculations it is worthwhile multiplying and dividing Eq. 46 by the secant radical.

$$K = \left[\frac{F_{s2} * Y + (1.025 - F_{s2}) * X}{\left[\sec\left(\frac{\pi\alpha}{2}\right) \right]^{1/2}} \right] * F_g * \frac{2}{\pi} * \sigma \sqrt{\pi a} * \left[\sec\left(\frac{\pi\alpha}{2}\right) \right]^{1/2} \quad (50)$$

3.4.3 Interpolation for Half-Elliptical Cracks ($0 \leq a/b \leq 1$)

An intermediate position between Eqs. 38 and 50 is necessary for half-elliptical crack shapes. Comparison of the two equations reveals that each contains the F_g factor and the secant radical. These are henceforth termed the combined stress gradient and back free surface correction factors, respectively. It is also apparent that each equation contains the appropriate, isolated, crack shape correction factor, F_e . ($F_e = 1.0$ is implied in Eq. 38.) Therefore,

use of the normal elliptical integral (Art. 3.1.1) for the combined crack shape correction is warranted. This integral automatically provides a nonlinear interpolation.

Only the leading bracketed expressions in each equation remain to be adjusted for half-elliptical crack shapes. While not precise, the simplest approach is a linear interpolation based on the crack shape ratio, a/b . The interpolated value represents the combined front free surface correction, F_s .

$$F_s = \left(1 - \frac{a}{b}\right) * \left\{ F_{s1} * C + (1.122 - F_{s1} * C) * X \right\} \quad (51)$$

$$+ \frac{a}{b} * \frac{F_{s2} * Y + (1.025 - F_{s2}) * X}{\left[\sec\left(\frac{\pi\alpha}{2}\right) \right]^{1/2}}$$

The combined stress intensity correction factors for stiffeners and cover plates are summarized in Table 5.

3.4.4 F_s Variation at Typical Details

The values of front free surface correction factor (Table 5) depend on detail type, detail geometry, crack shape, and crack depth. In order to indicate the trend at typical details, a sample stiffener geometry was selected. The geometry consisted of a one-inch flange and a 5/16 inch weld leg. The resulting variations of F_s with α are plotted in Fig. 20.

It is apparent that the crack shape is of major importance to the value of F_s for stiffeners. The more half-circular the crack shape, the lower F_s . However, even with a constant shape, F_s decays as α increases. The decay is more rapid for shapes nearer the half-circle. These characteristics are also valid for cover plate details.

4. FATIGUE LIFE CORRELATIONS

The correction factors developed in Chapter 3 (Table 5) can be used in fatigue life predictions. After replacing stress, σ , with stress range, S_r , in the stress intensity expressions, the resulting range of stress intensity is inserted in Eq. 2. It is rare that this equation can be solved closed-form - particularly when the combined correction factor, CF, is a complicated function of crack length, a . Therefore, the cycle life is commonly estimated on the basis of the following numerical integration:

$$N = \frac{1}{C} \sum_{j=1}^m \frac{1}{(\Delta K_j)^n} \Delta a_j \quad (52)$$

where $C_1 = 2.0 \cdot 10^{-10} \frac{\text{in.}^{11/2}}{\text{kip}^3 \text{ cycles}}$ mean (Refs. 10, 17)

$C_2 = 3.6 \cdot 10^{-10} \frac{\text{in.}^{11/2}}{\text{kip}^3 \text{ cycles}}$ upper bound (Ref. 39)

ΔK = range of stress intensity, ksi $\sqrt{\text{in.}}$

Δa = crack length increment, in.

A sense of the relative importance of stress range and initial and final crack sizes in life estimates may be developed by again considering Eq. 2. If the combined correction factor is assumed (for this exercise) to be constant, the cycle life is predictable in closed-form fashion.

$$N = \frac{2}{C \cdot CF^3 \cdot S_r^3 \cdot \pi^{3/2}} \left[a_i^{-1/2} - a_f^{-1/2} \right] \quad (53)$$

where a_i = initial crack size
 a_f = final crack size

Since stress range is cubed and both crack lengths have a square root sign attached, error in the nominal stress range is much more important than errors in the initial and final crack sizes. Likewise, error in the correction factor, CF, is more important than crack size. Even though CF in reality depends on crack size, added importance is obviously attached to establishment of the correct form of each individual correction factor.

The negative radical associated with each crack length typically places the weighted importance on initial crack size. Experimental work outlined in Refs. 9 and 10 used an excessive deflection (net section yielding) criterion for fatigue failure and the establishment of a_f . A more recent study terminated fatigue life with fracture, although this life was close to that found using a generalized yielding condition.⁽⁷⁾ Both definitions of failure generally cause a_f to be much larger than a_i . The greater the difference between a_i and a_f , the greater the importance of a_i .

In light of the relative importance of a_i , it is indeed unfortunate that a_i is much more difficult to estimate than a_f . Such is even true

for a test specimen where the crack surface is exposed after failure (a_f is usually clearly evident). Nevertheless, several investigations have established lower and upper limits of initial crack size for weld toes of a stiffener or cruciform joint at about 0.003 in. and 0.02 in., respectively. (31,36) The average a_i is between .003 in. and .004 in.

Given the expression for stress intensity and information on initial crack sizes, the analyst is in a position to make fatigue life (cycle) estimates. Several sample details are subsequently investigated and their lives are compared with those found under actual fatigue test conditions. Since stiffener and cover-plated beams had welds that were perpendicular to the stress field, it was assumed that the fatigue cracks coalesced. Hence Eqs. 23 and 26 were used to describe the crack shape relationship for the analysis described hereafter.

4.1 Transverse Stiffeners Fillet-Welded to Flanges

Reference 10 provides a broad experimental base for fatigue failure at stiffeners. Stiffeners fillet-welded to flanges are therein designated Type 3. One particular series (in this case the SGB-SBB combined series) is selected for investigation and values of the crucial geometric variables are tabulated in Table 6. (Appendix E of Ref. 10 notes that the actual weld size was closer to 0.25 in. rather than the 0.1875 in. dimension specified.) The objective is to assess how accurately the result of the estimate approach, N_{est} , predicts the actual cycle life, N_{act} . All lives are also recorded in Table 6.

The actual cycle life in Table 6 relates to the logarithmic average of data points for the given series and stress range (Table E-3 of Ref. 10). Logarithmic average means that variable N is assumed log-normally distributed (base 10) and the mean is approximated by the average logarithm of the data points. For this particular series and stress range, eight data points are available. On average, failure occurred after the crack had fully penetrated the flange and was growing in a through crack configuration. Since the life estimates are based on cycle life for growth through the flange, 96 percent of the actual life found by the logarithmic average is recorded.

Four estimated lives were derived from the stress intensity relationships (Table 5). They represent approximate average and maximum initial crack sizes and crack growth rates. In comparison with N_{act} (average) in Table 5, it is seen that the theoretical results all provide life estimates that are conservative. The results are also plotted in Fig. 21 and compared with the results of regression analyses of all of the test data. It is probable that Eq. 25 represents a more reasonable crack shape relationship for transverse stiffener details. The use of Eq. 26 provides a more severe condition.

Reference 10 provides two regression equations which can be used to estimate life. The mean equation for all stiffeners (not just those connected to the flange) is as follows:

$$\log N = 10.0852 - 3.097 \log S_r \quad (54)$$

Since 96 percent of N is to be used for comparison purposes, Eq. 54 can be modified accordingly.

$$\log (.96N) = 10.0675 - 3.097 \log S_r \quad (55)$$

The mean equation for Type 3 stiffeners only (all series) is:

$$\log N = 10.5949 - 3.505 \log S_r \quad (56)$$

For 96 percent of N the regression equation appears as follows:

$$\log (.96N) = 10.5772 - 3.505 \log S_r \quad (57)$$

It is noted that neither regression equation has a slope of exactly -3.0. However, the discrepancy is minor. In fact, the estimates by Eq. 54 and 56 or 55 and 57 are normally quite close due to the adjustment provided by the equation constants (Fig. 21). A common slope of -3.0 guided the AASHTO Specifications⁽²⁾ although round off of stress range values left the slope slightly off of the mark. Regardless, equating n to 3.0 is reasonable in the life integral procedure (Eq. 52).

Since both of the above regression equations are based upon the specific series under study here, close agreement between predicted and actual cycle life is expected and, indeed, found (Table 6 and Fig. 20). However, it is also fruitful to compare the value at the (approximate) upper 95 confidence limit. Again assuming log-normal distribution and

incorporating the standard deviation ($s = 0.1024$) from the Type 3 regression analysis, Eq. 57 is adjusted to the upper 95 percent confidence limit.

$$\begin{aligned}\log (.96N) &= 10.5772 - 3.505 \log S_r + 2s & (58) \\ &= 10.7820 - 3.505 \log S_r\end{aligned}$$

The large separation between the upper confidence limit and the mean value emphasizes the wide variability of experimental data. This separation thereby gives a measure of accuracy of the unified estimate at the average initial crack size.

4.2 Cover Plates With Transverse End Welds

Reference 9 is a source of considerable data on cover plates. Combined series CWB-CWC was selected for investigation and the important geometrical parameters are summarized in Table 6. (Series CWA had a slightly different flange thickness, Table D-2 of Ref. 9, and was therefore omitted from the combination.) The stress range assumed is 16 ksi. Thus, using the logarithmic average of the twelve available data points (Tables F-2 and F-3 of Ref. 9), the 96 percent life is set at 0.356 million cycles.

The life estimates for the average and maximum initial crack sizes and crack growth rates are given in Table 6 and Fig. 22. The estimates

given in Table 6 bound the average life N_{act} for both crack growth rates. The results plotted in Fig. 22 are compared with the results of regression analyses of all of the test data.

Reference 9 gives the following regression equation for all cover plates with transverse end welds:

$$\log N = 9.2920 - 3.095 \log S_r \quad (59)$$

Incorporation of the 96 percent life for crack growth through the flange modifieds Eq. 59 as follows:

$$\log (.96N) = 9.2743 - 3.095 \log S_r \quad (60)$$

For the specific stress range in Table 6, it can be seen that the estimated life from Eq. 60 (by chance) precisely equals the actual life for the particular series being studied. By making use of the standard error for Eq. 59 ($s = 0.101$), it is again possible to define the equation for the upper 95 percent confidence limit.

$$\begin{aligned} \log (.96N) &= 9.2743 - 3.095 \log S_r + 2s & (61) \\ &= 9.4763 - 3.095 \log S_r \end{aligned}$$

Equations 60 and 61 are plotted in Fig. 22. Reasonable agreement is seen to exist between the predicted fatigue life and the experimental results.

The minimum and maximum life estimates correlate well with the lower and upper confidence limits of the test data.

It is apparent from this analysis that the crack shape relationship and the crack growth rate both have a significant effect on the fatigue life estimate. It seems reasonable to expect the wide variation in fatigue life that is experienced in laboratory studies considering the random nature of initial crack size, stress concentration conditions and crack growth rates that are known to exist.

5. SUMMARY AND CONCLUSIONS

In this report the stress concentration effects on fatigue cracks that grow at weld terminations has been investigated. Finite element studies were used to develop the stress concentration factor decay curves for stiffener and cover plate details. These results were then used to express the stress concentration conditions in terms of joint geometry and weld size.

To permit a fatigue life analysis of typical welded details, the total stress intensity at the weld toe was developed including the stress gradient correction factor, the crack shape correction, the front free surface correction and the back free surface correction. These correction factors were used together with a lower bound crack shape relationship to estimate the fatigue life of transverse stiffeners welded to the flange and cover-plated beams with transverse end welds using the Paris power law.

The results of the analyses were compared with the experimental results reported in NCHRP Reports 102⁽⁹⁾ and 147⁽¹⁰⁾. Good agreement was experienced between the predicted fatigue life and the experimental test data. When extreme conditions of initial crack size and crack growth rate were assumed, the predicted life fell near or below the lower confidence limit of the test data. When the average crack size and crack growth rate

were used, the predicted life was between the mean and upper confidence limits.

The correlation of the analyses and experimental data indicate that the model can provide a useful tool for estimating the crack growth behavior of other welded details.

6. TABLES

TABLE 1

Decay Constants of Approximate Stress Concentration and
Stress Gradient Correction Factor Curve Formulas

$$\frac{K_t \lambda}{SCF} \approx \frac{1}{1 + \frac{1}{c} \lambda^p}$$

$$\frac{F_{g\alpha}}{SCF} \approx \frac{1}{1 + \frac{1}{d} \alpha^q}$$

Constant	Stiffener	Cover Plate
c	0.3546	0.1159
p	0.1543	0.3838
d	0.3602	0.1473
q	0.2487	0.4348


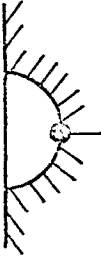
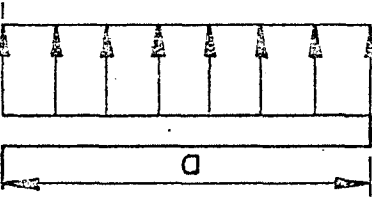
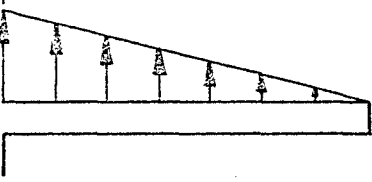
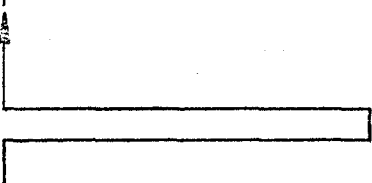
<div style="display: flex; justify-content: space-between;"> <div style="width: 45%; text-align: center;">STRESS DISTRIBUTION</div> <div style="width: 55%; text-align: center;">CRACK SHAPE</div> </div>		
	1.122	1.025
	1.210	1.085
	1.300	~ 1.145

Table 2 Front Free Surface Correction Factor for Various Crack Shapes and Stress Distribution (28, 32, 34, 35)

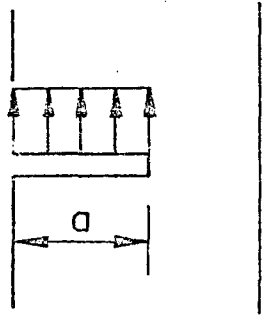
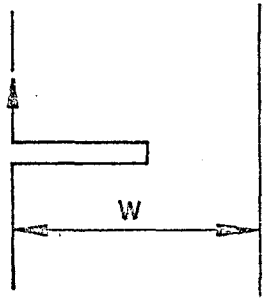
STRESS DISTRIBUTION	NO BENDING	BENDING
	$\left[\sec \left(\frac{\pi\alpha}{2} \right) \right]^{1/2}$ $\alpha = \frac{a}{w}$	$\left[\frac{0.752 + 2.02\alpha + 0.37 \left[1 - \sin \left(\frac{\pi\alpha}{2} \right) \right]^3}{1.122 \cos \left(\frac{\pi\alpha}{2} \right)} \right]$ $* \left[\frac{2}{\pi\alpha} \sin \left(\frac{\pi\alpha}{2} \right) \right]^{1/2}$ $* \left[\sec \left(\frac{\pi\alpha}{2} \right) \right]^{1/2}$
	$\left[1.297 - 0.297 \cos \left(\frac{\pi\alpha}{2} \right) \right]$ $* \left[\frac{\pi\alpha}{2} \operatorname{cosec} \left(\frac{\pi\alpha}{2} \right) \right]^{1/2}$ $* \left[\sec \left(\frac{\pi\alpha}{2} \right) \right]^{1/2}$	$\left[\frac{3.52}{(1-\alpha)^{3/2}} - \frac{4.35}{(1-\alpha)^{1/2}} + 2.13 (1-\alpha) \right]$ $* \frac{1}{1.30} \left[\cos \left(\frac{\pi\alpha}{2} \right) \right]^{1/2}$ $* \left[\sec \left(\frac{\pi\alpha}{2} \right) \right]^{1/2}$

Table 3 Back Free Surface Correction Factor for Through Cracks with Various Stress Distributions and Bending Conditions (28, 32, 34, 35)

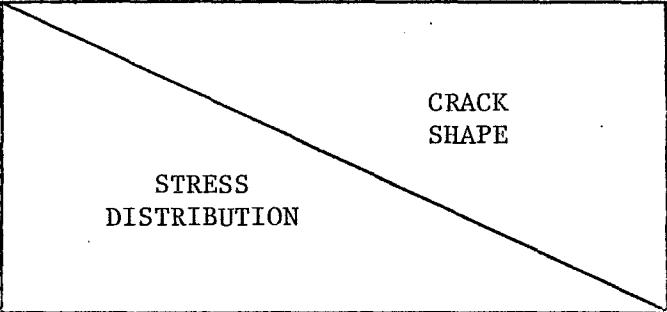
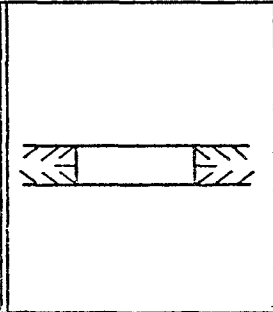
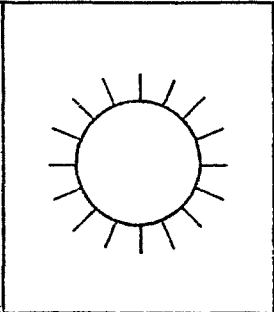
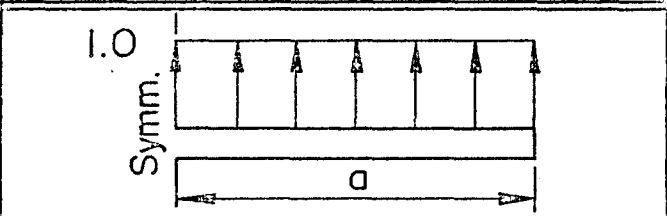
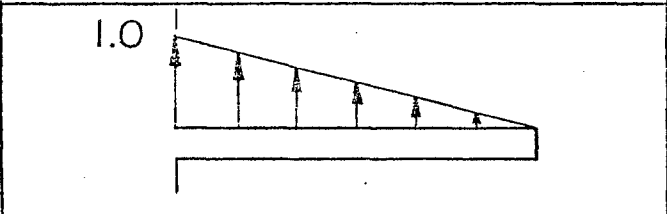
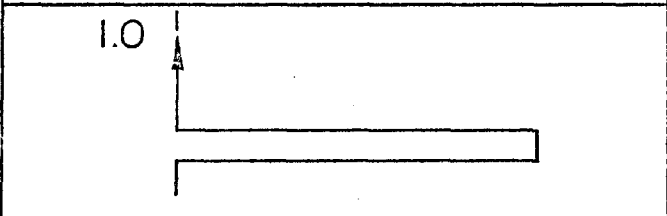
			RATIO Y
	1.000	1.000	1.000
	0.363	0.281	0.774
			~0.548

Table 4 Comparison of Stress Gradient Correction Factors for Various Crack Shapes and Stress Distributions (1, 35)

TABLE 5

Summary of Combined Correction Factors for
Stress Intensity Expression for Stiffeners and Cover Plates

Front Free Surface, F_s	$\left(1 - \frac{a}{b}\right) \left\{ F_{s1} * C + (1.122 - F_{s1} * C) * X \right\} + \frac{a}{B}$ $* \left\{ \frac{F_{x2} * Y + (1.025 - F_{s2}) * X}{\left[\sec\left(\frac{\pi Q}{2}\right) \right]^{1/2}} \right\}$
Crack Shape, F_e	$\frac{1}{E(k)}$
Back Free Surface, F_w	$\left[\sec\left(\frac{\pi Q}{2}\right) \right]^{1/2}$
Stress Gradient, F_g	<p>as evaluated by the correlated stress decay from an elliptical hole in an infinite plate</p>

TABLE 6

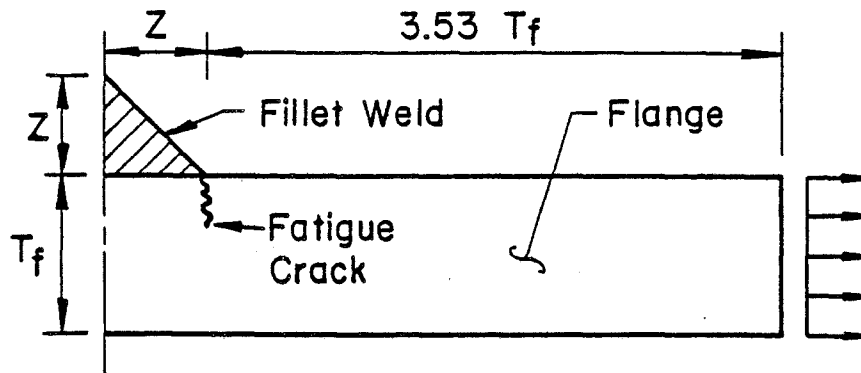
Cycle Life Comparisons for
Sample Stiffener and Coverplate Details

Detail	S_r [ksi]	T_f [in]	Z [in]	T_{cp} [in]	N_{act}^*	N_{est}^* $C=2*10^{-10**}$	N_{est}^* $C=3.6*10^{-10**}$
Stiffener Fillet-Welded to Flange	18.4	0.50	0.25		1.346	1.304 ($a_i=0.003''$)	0.724 ($a_i=0.003''$)
(Ref. 10, Series SGB-SBB)						0.919 ($a_i=0.02''$)	0.511 ($a_i=0.02''$)
Coverplate with Transverse End Weld	16.0	0.393	0.25	0.55	0.356	0.492 ($a_i=1.003''$)	0.274 ($a_i=.003''$)
(Ref. 9, Series CWB, CWC)						0.430 ($a_i=0.02$)	0.239 ($a_i=.02$)

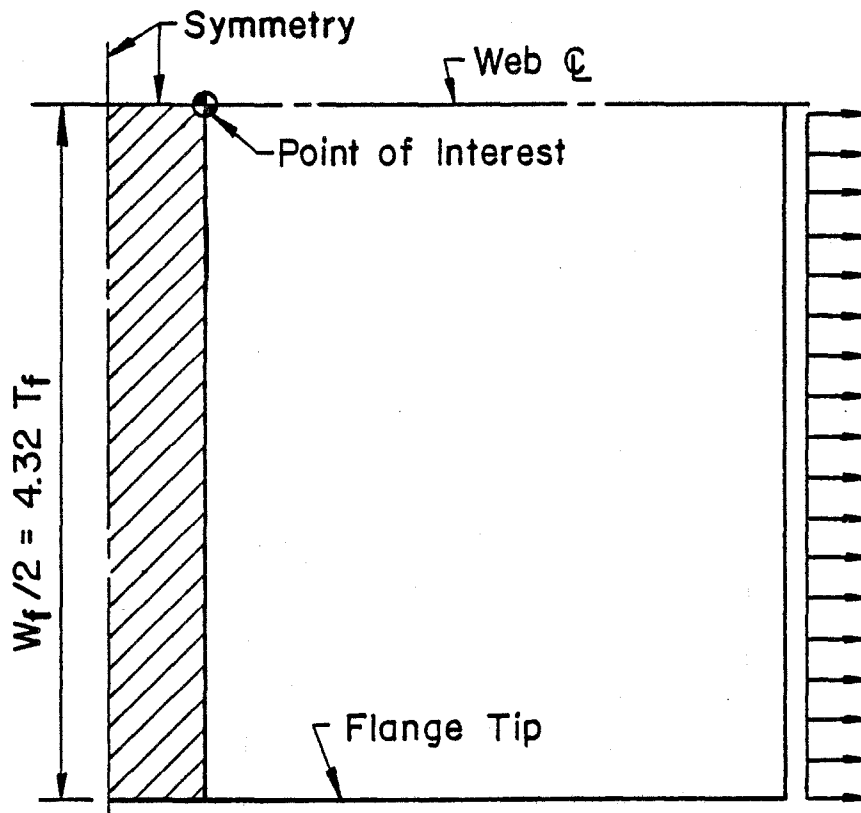
*All cycle lives in millions

** $\frac{in^{11/2}}{kip^3}$ cycles

7. FIGURES



a) Section



b) Plan View

Fig. 1 Detail Geometry for Transverse Stiffener Investigation

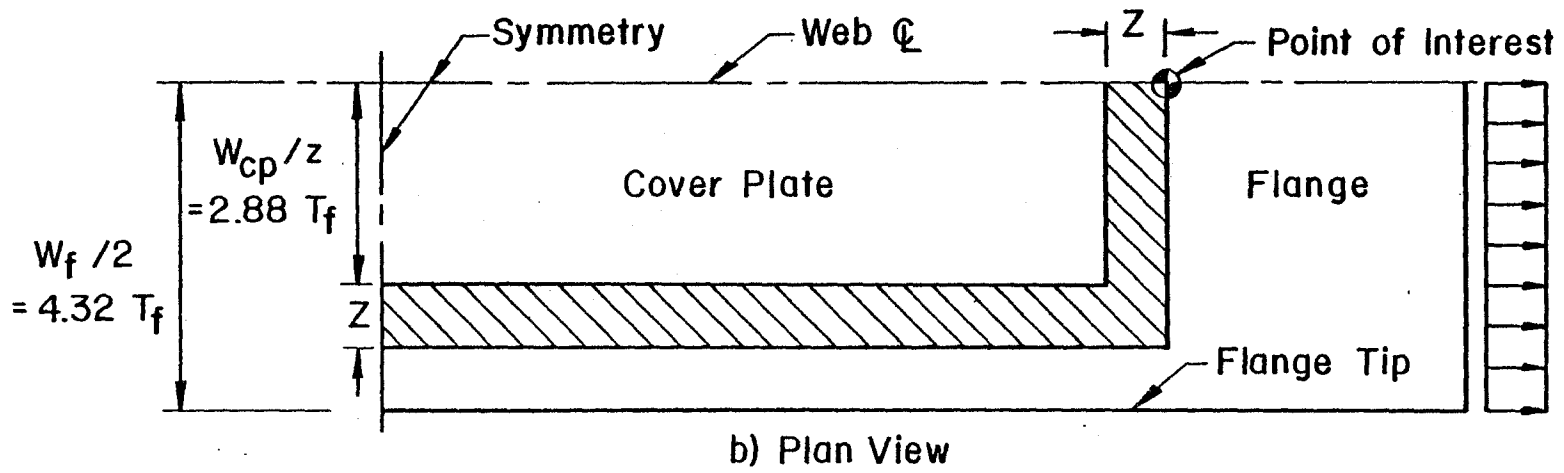
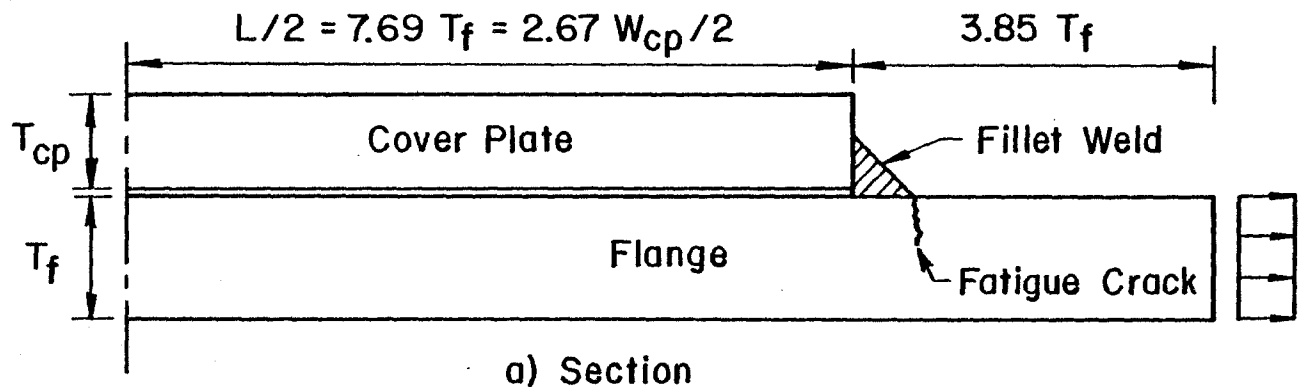
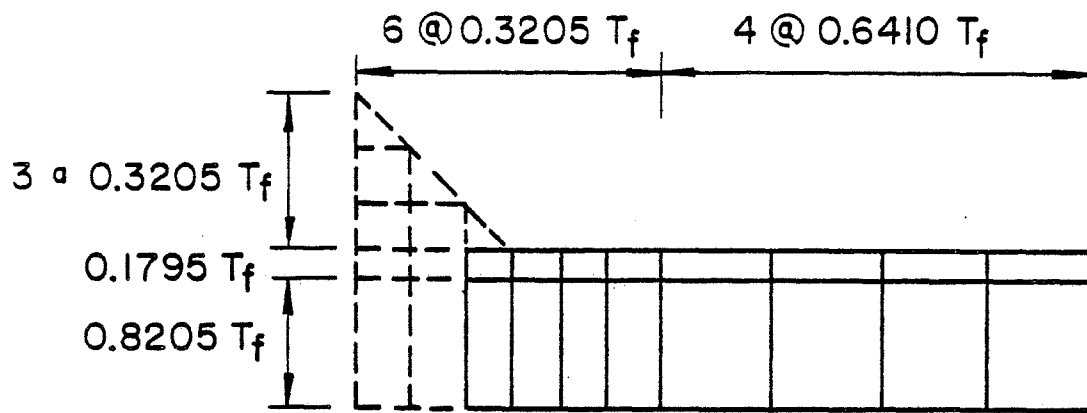
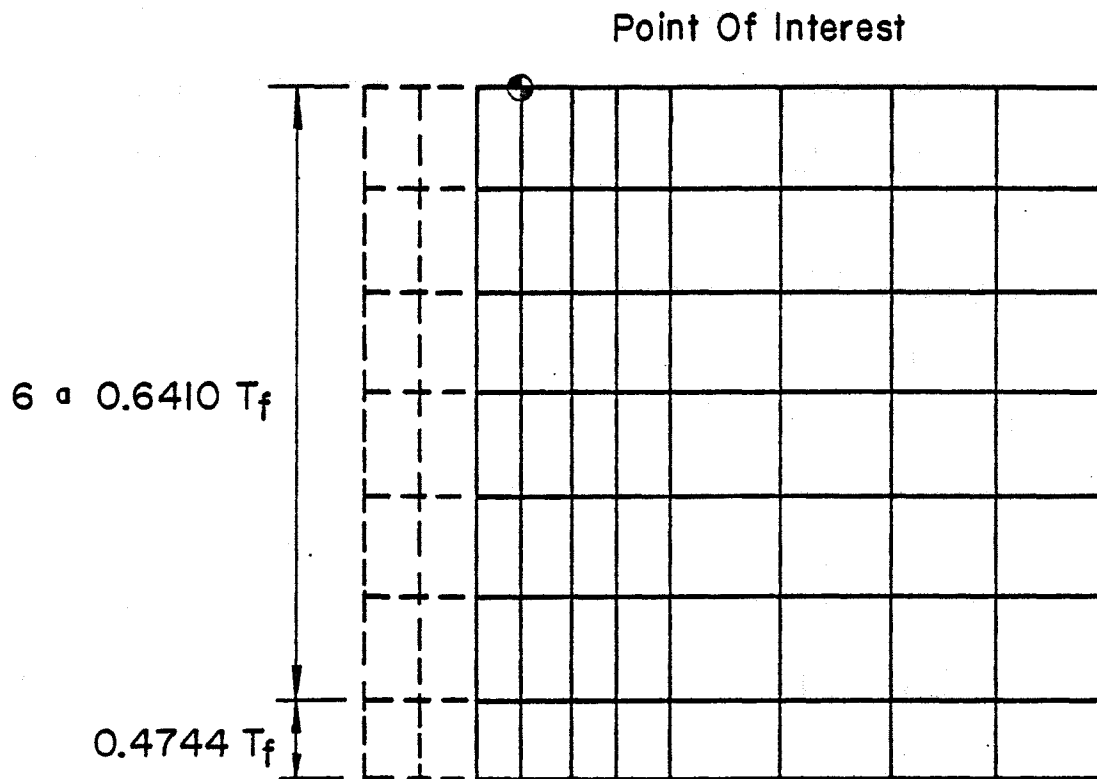


Fig. 2 Detail Geometry for Cover Plate Investigation



a) Section



b) Plan View

Fig. 3 Coarse Mesh for Transverse Stiffener Investigation

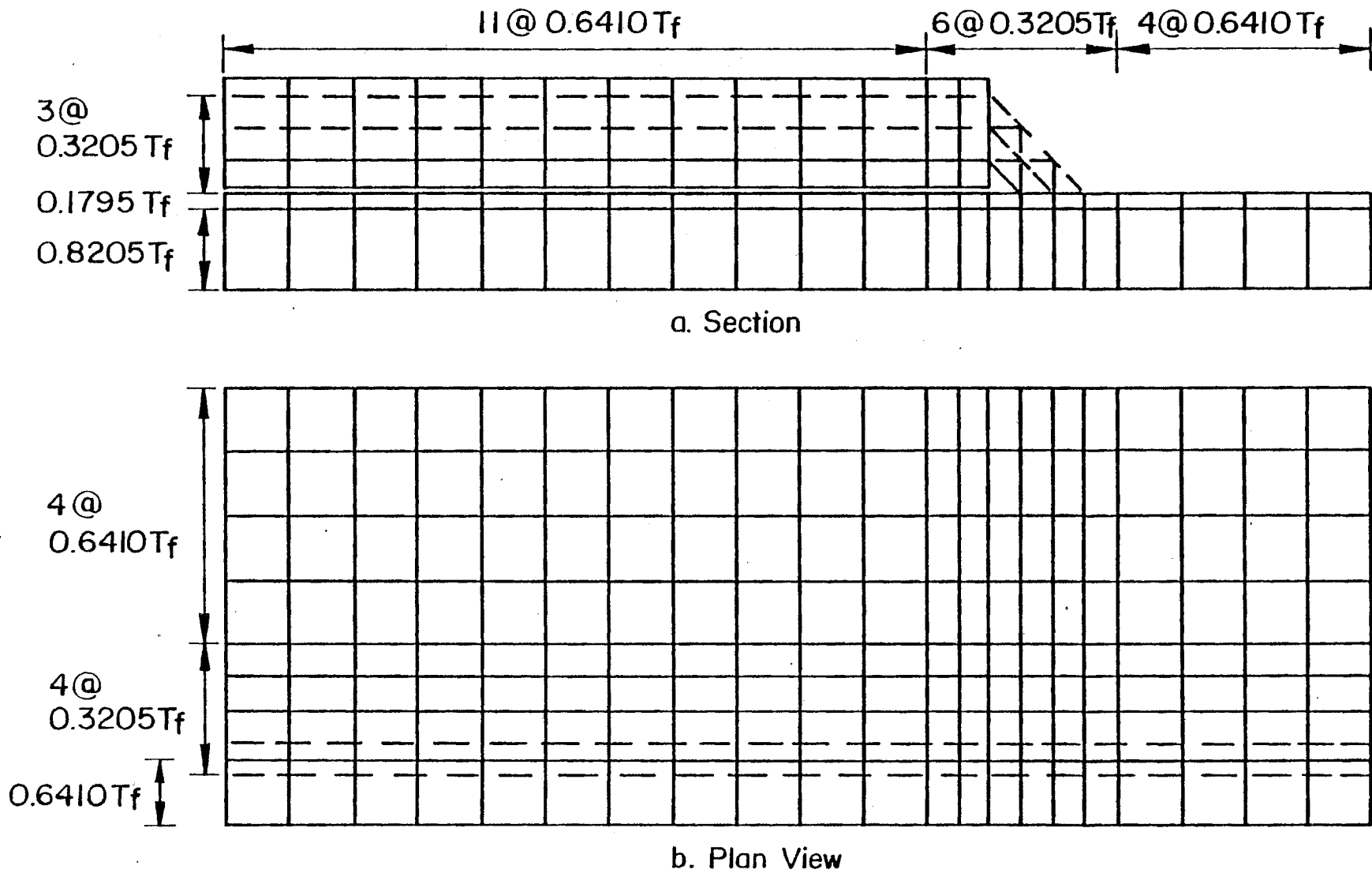


Fig. 4 Coarse Mesh for Cover Plate Investigation

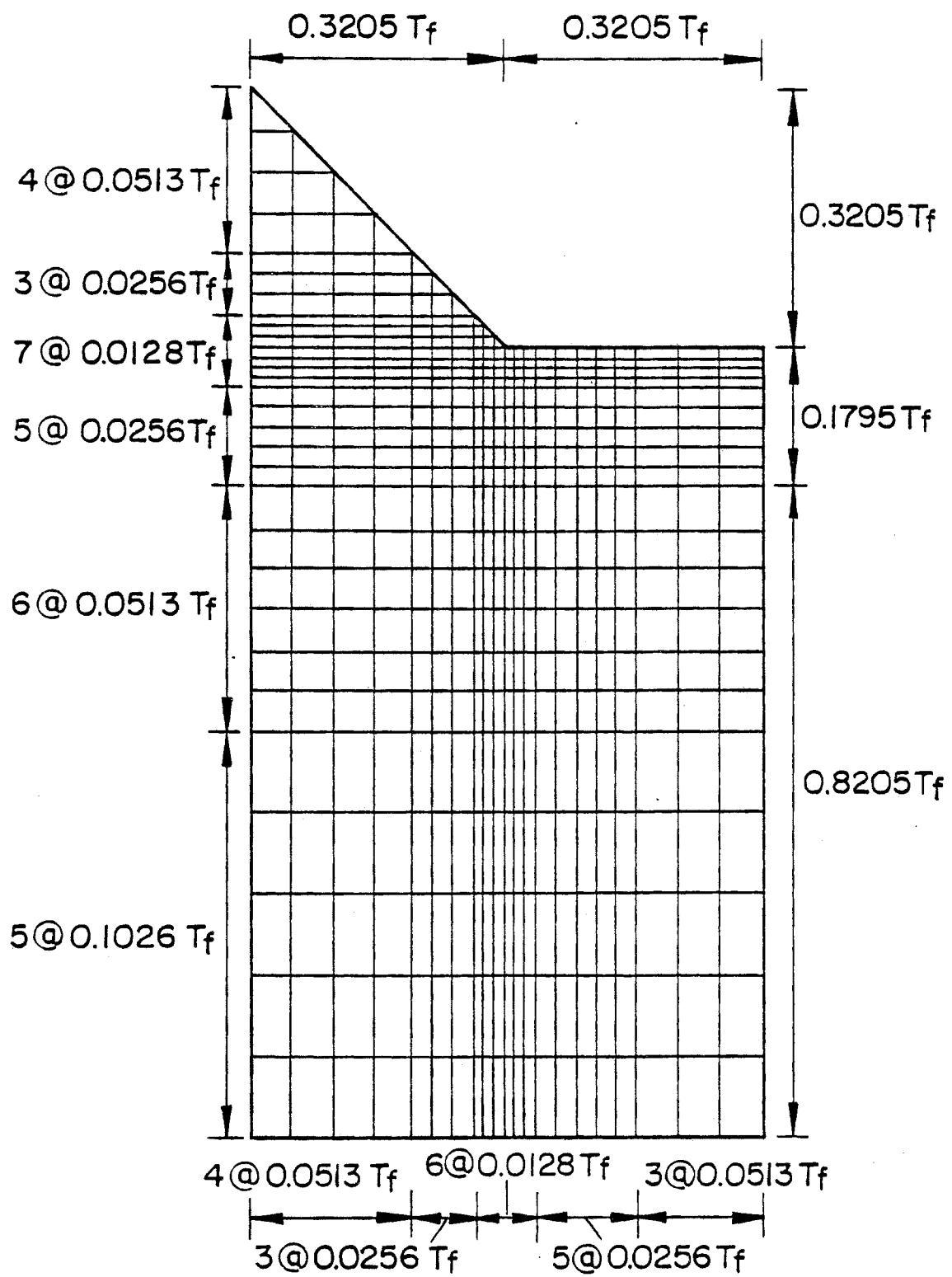


Fig. 5 Fine Mesh for Stiffener and Cover Plate Investigations

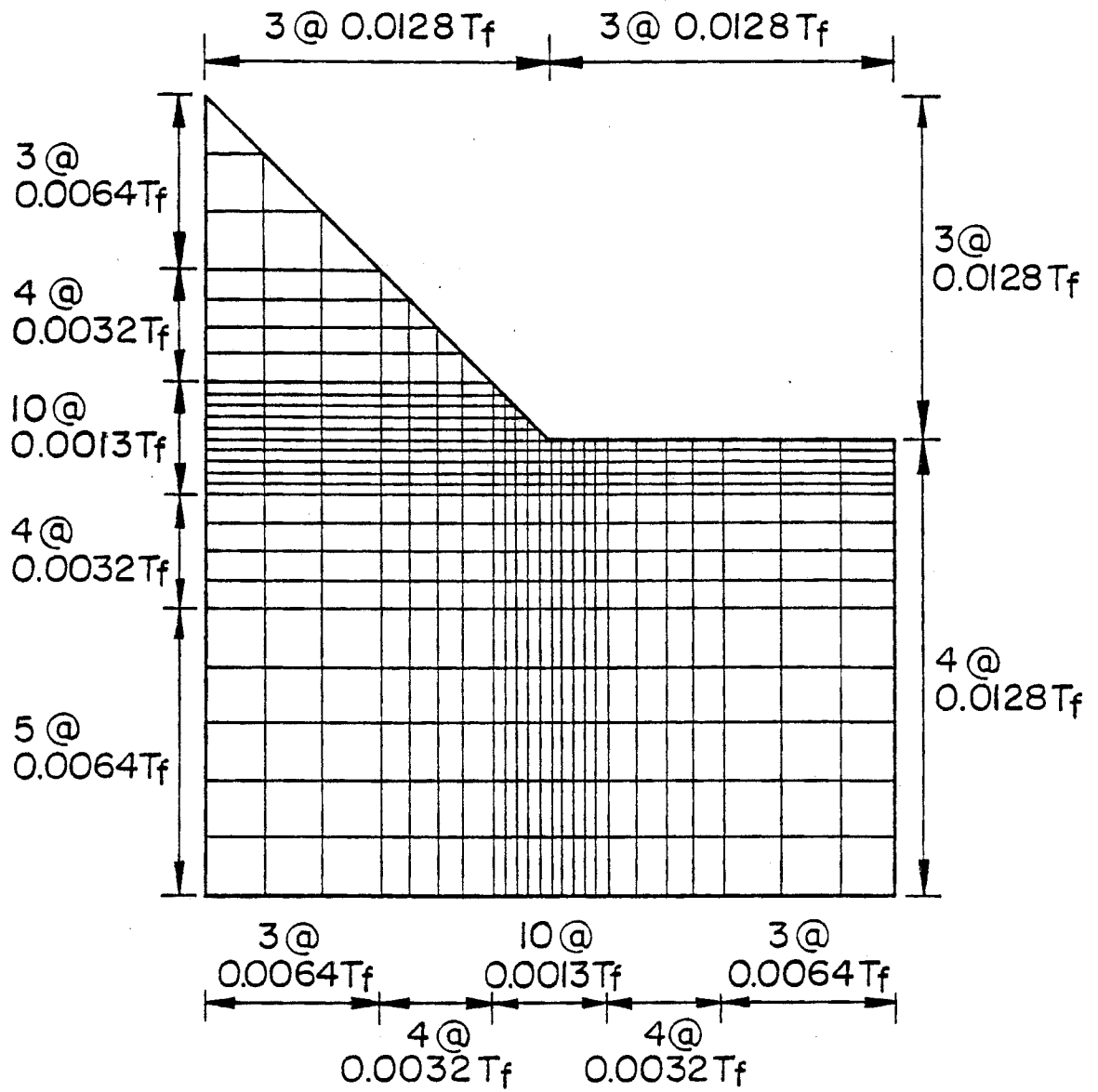


Fig. 6 Ultra Fine Mesh for Stiffener and Cover Plate Investigations

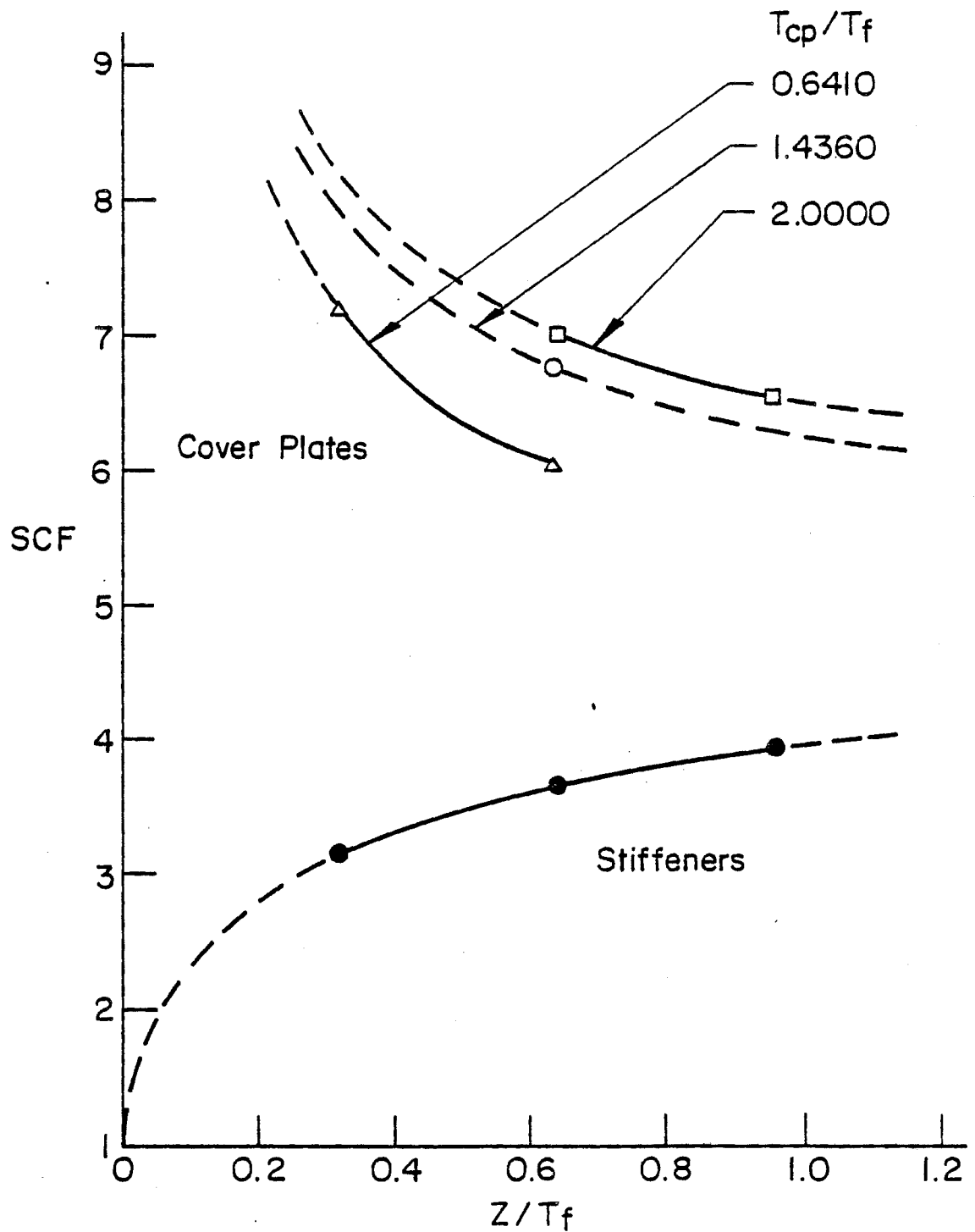


Fig. 7 Variation of Maximum Stress Concentration Factor with Weld Size at Stiffener and Cover Plate Details

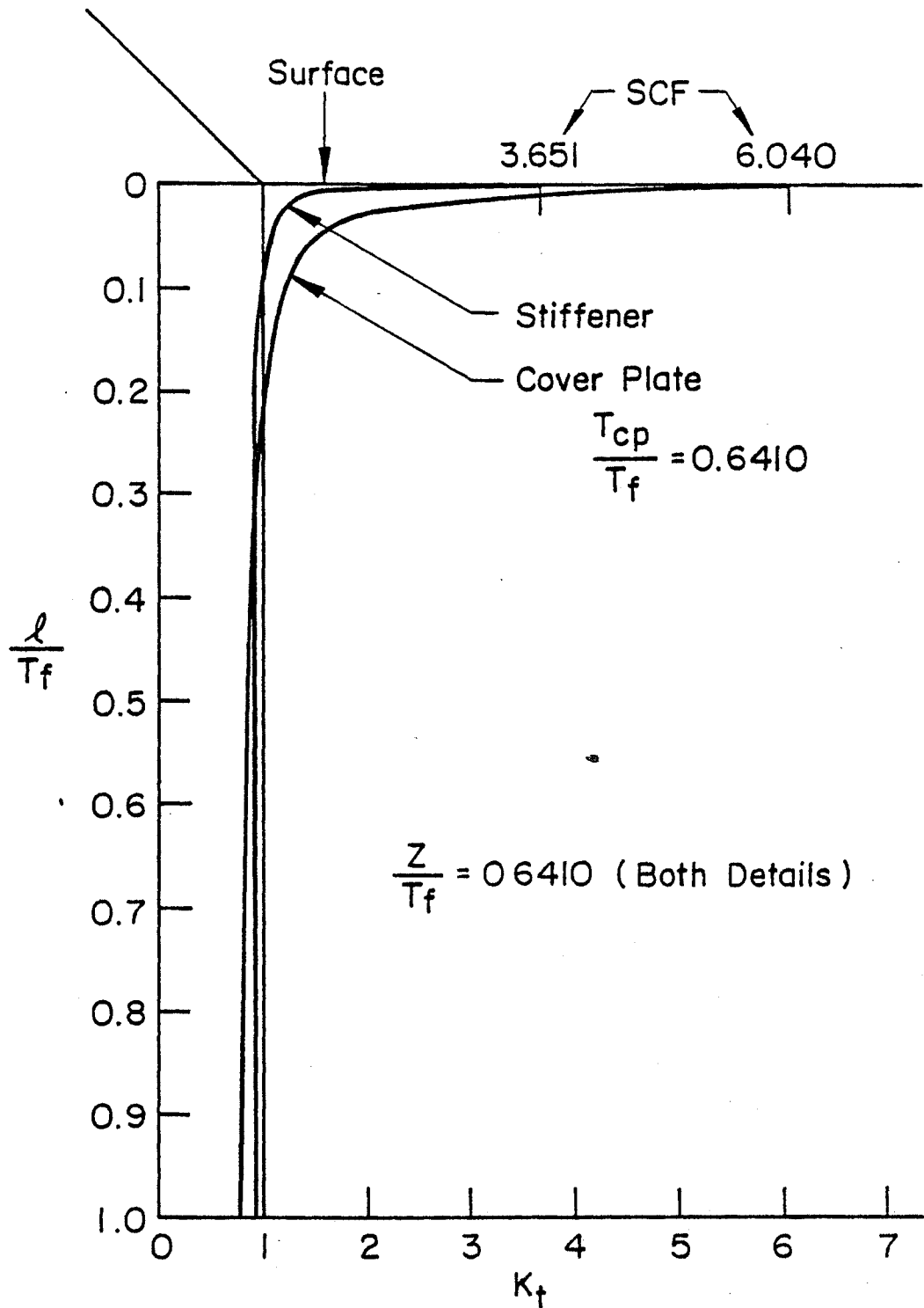


Fig. 8 Stress Concentration Factor Decay from Weld Toe through Flange Thickness at Sample Stiffener and Cover Plate Details

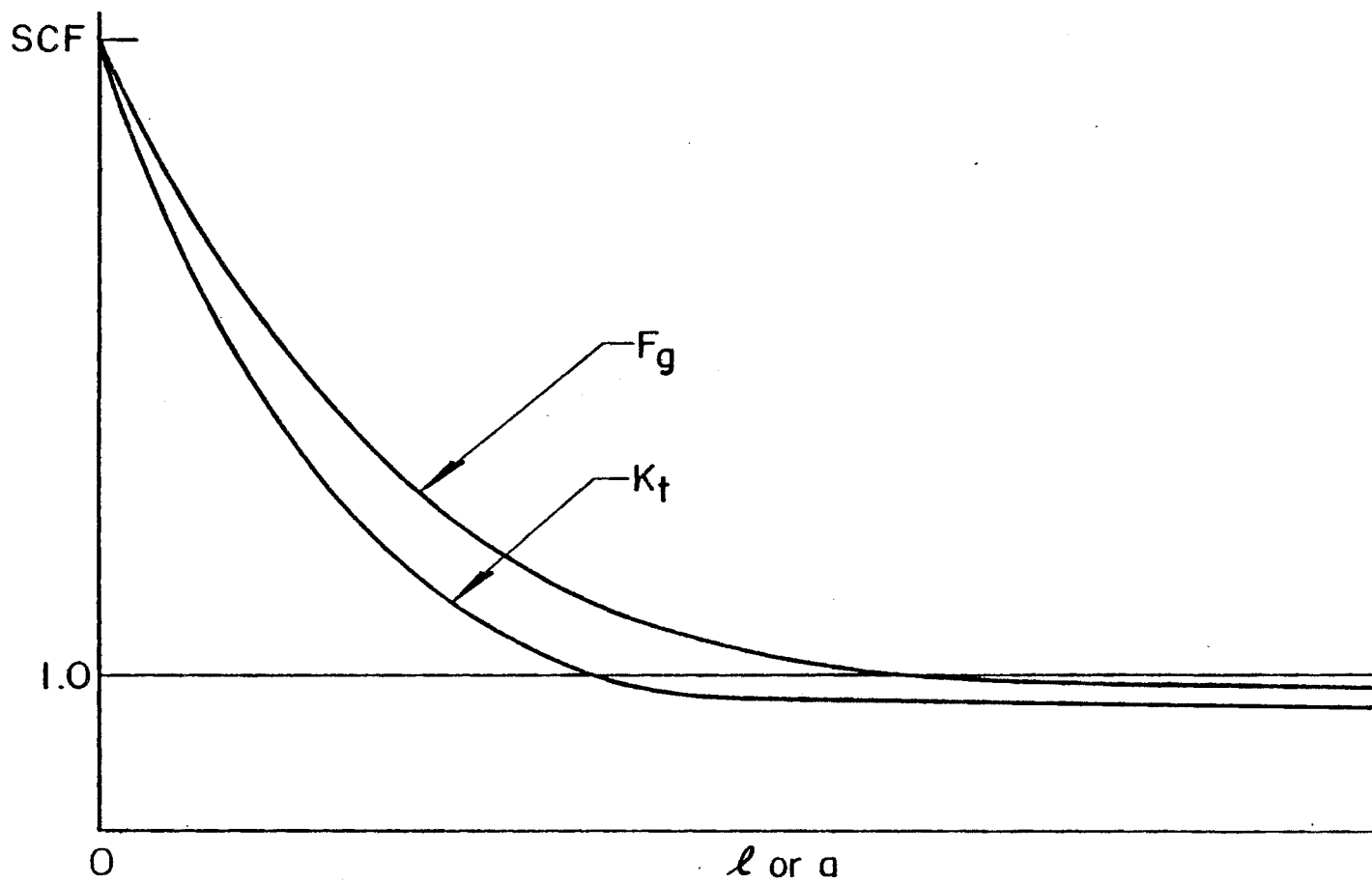


Fig. 9 Schematic Stress Concentration and Stress Gradient Correction Factor Decay Curves for Typical Welded Details

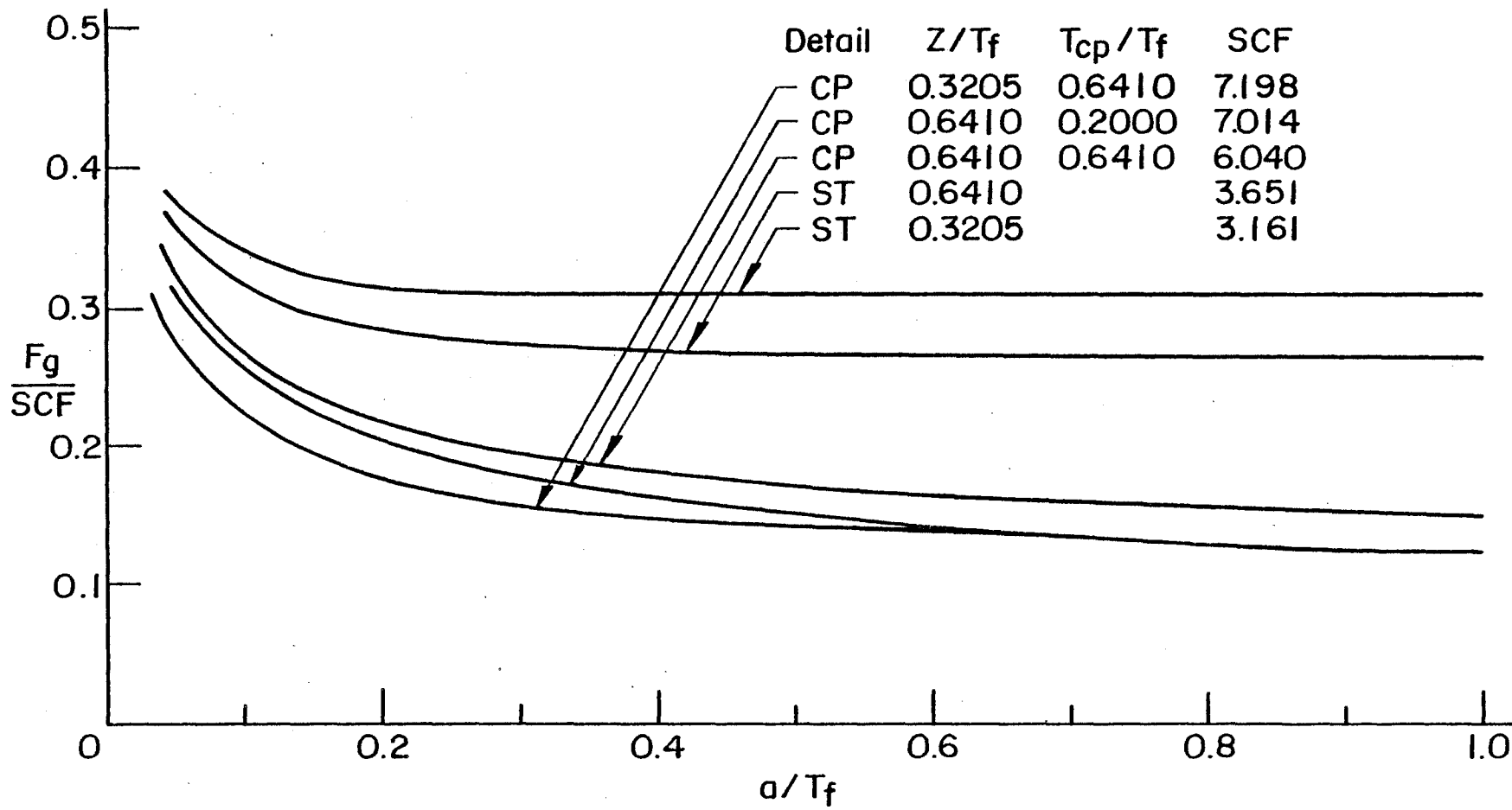


Fig. 10 F_g Decay Curves for Sample Stiffener and Cover Plate Details

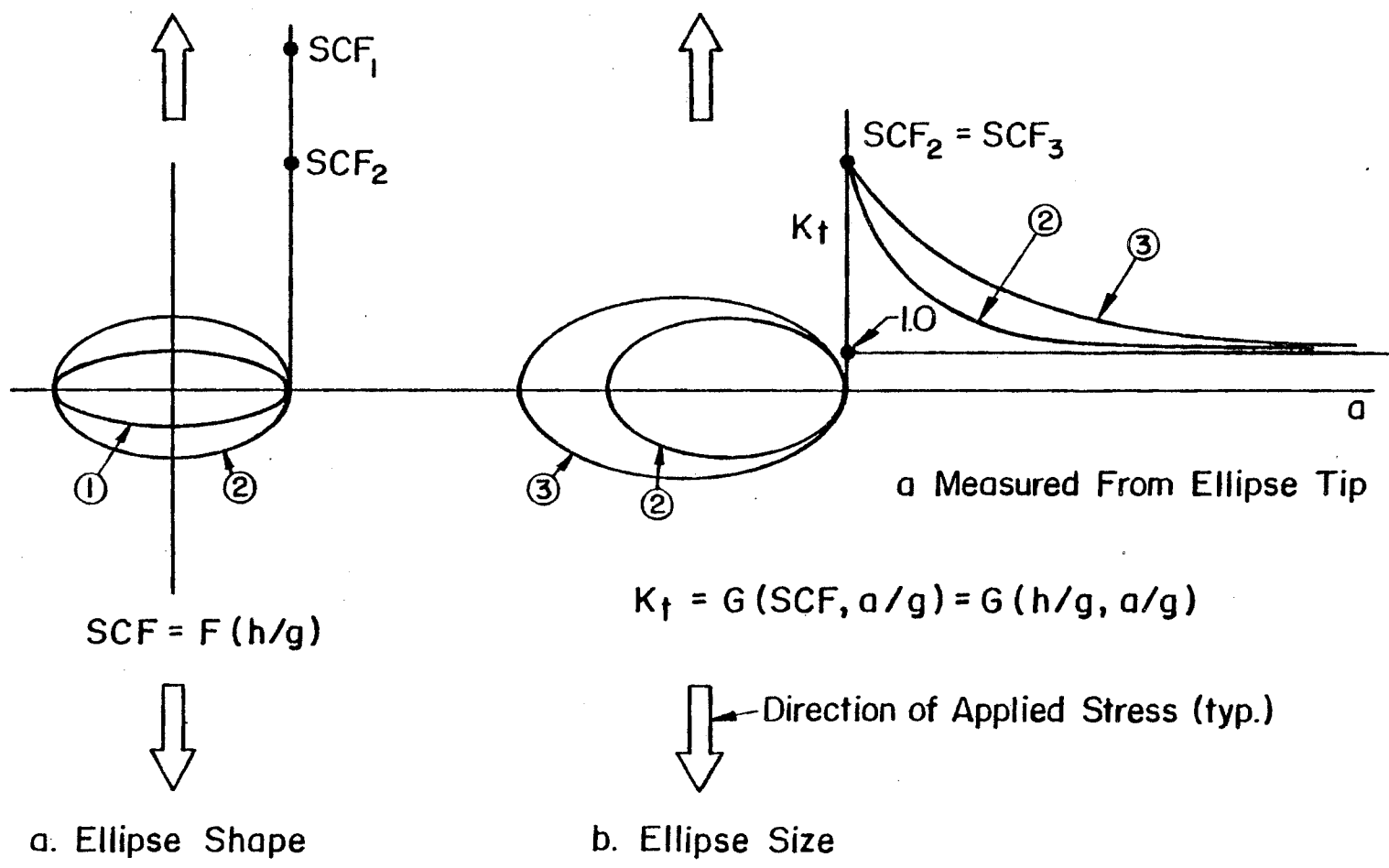


Fig. 11 Two Steps Required for Ellipse Correlation

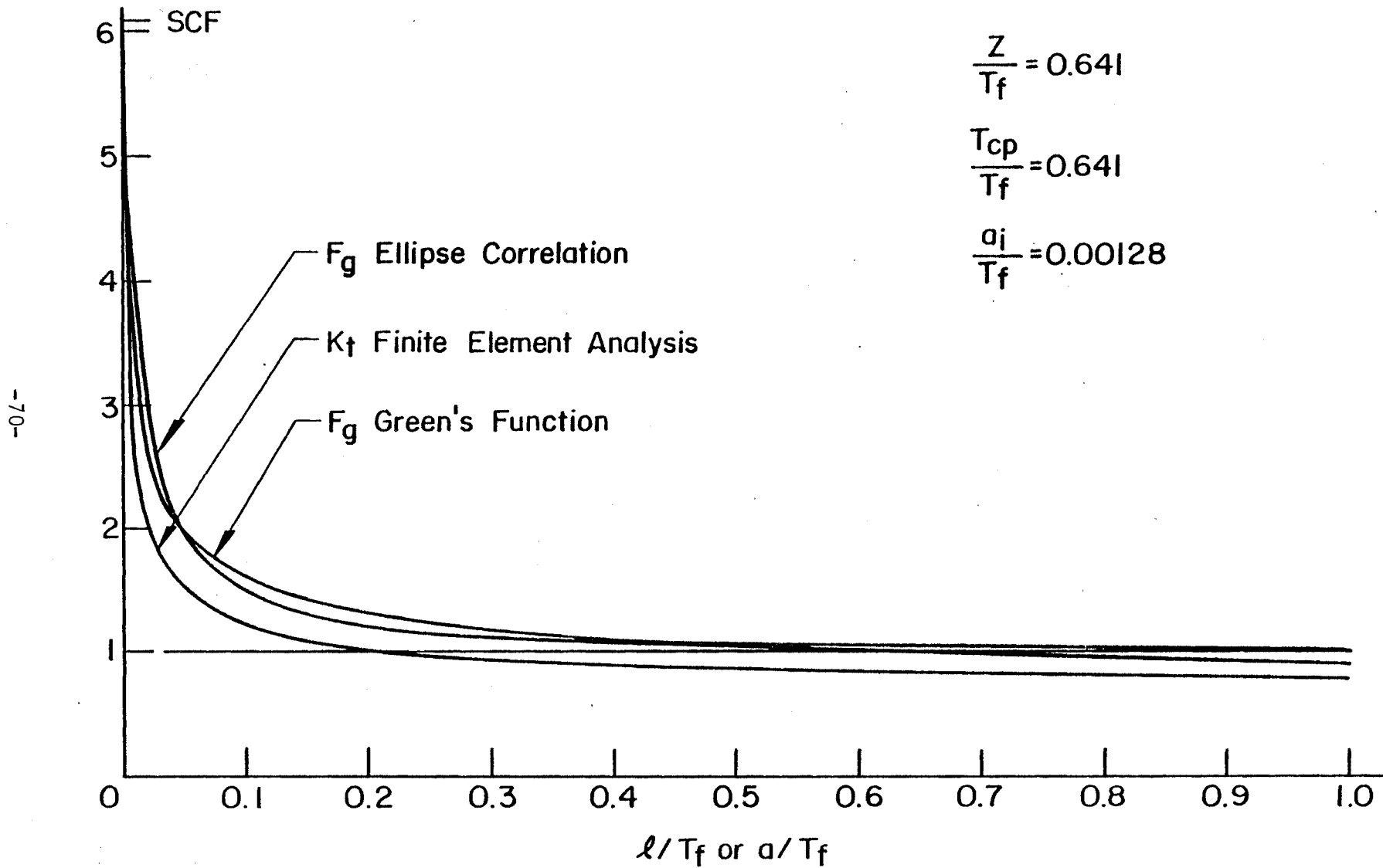


Fig. 12 Comparison of K_t and F_g Decay Curves for Sample Cover Plate Detail

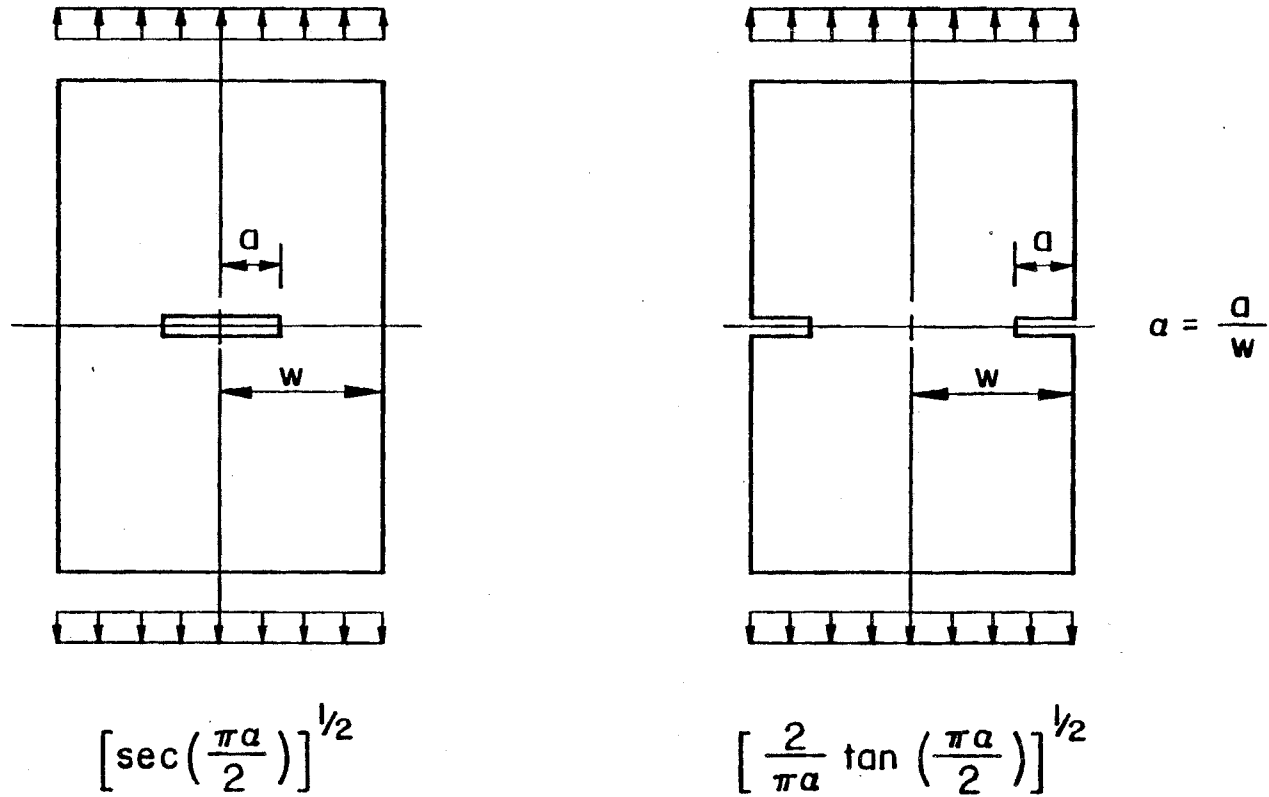
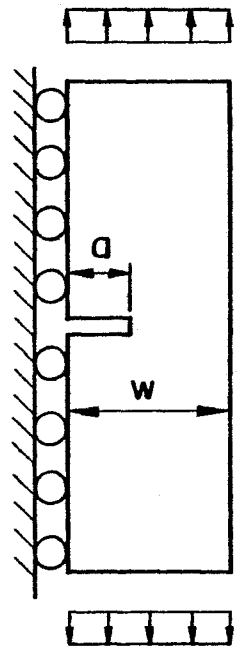
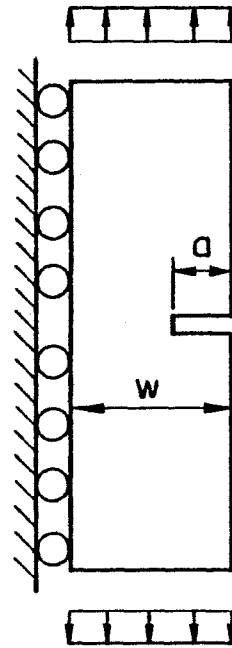


Fig. 13 Back Free Surface Correction Factor for Two Symmetrical Through Crack Configurations (17,20,22,23)



$$\left[\sec \left(\frac{\pi a}{2} \right) \right]^{1/2}$$



$$\left[\frac{2}{\pi a} \tan \left(\frac{\pi a}{2} \right) \right]^{1/2}$$

$$a = \frac{a}{w}$$

Fig. 14 Back Free Surface Correction Factor for Two Nonsymmetrical Through Crack Configurations with Bending Prevented

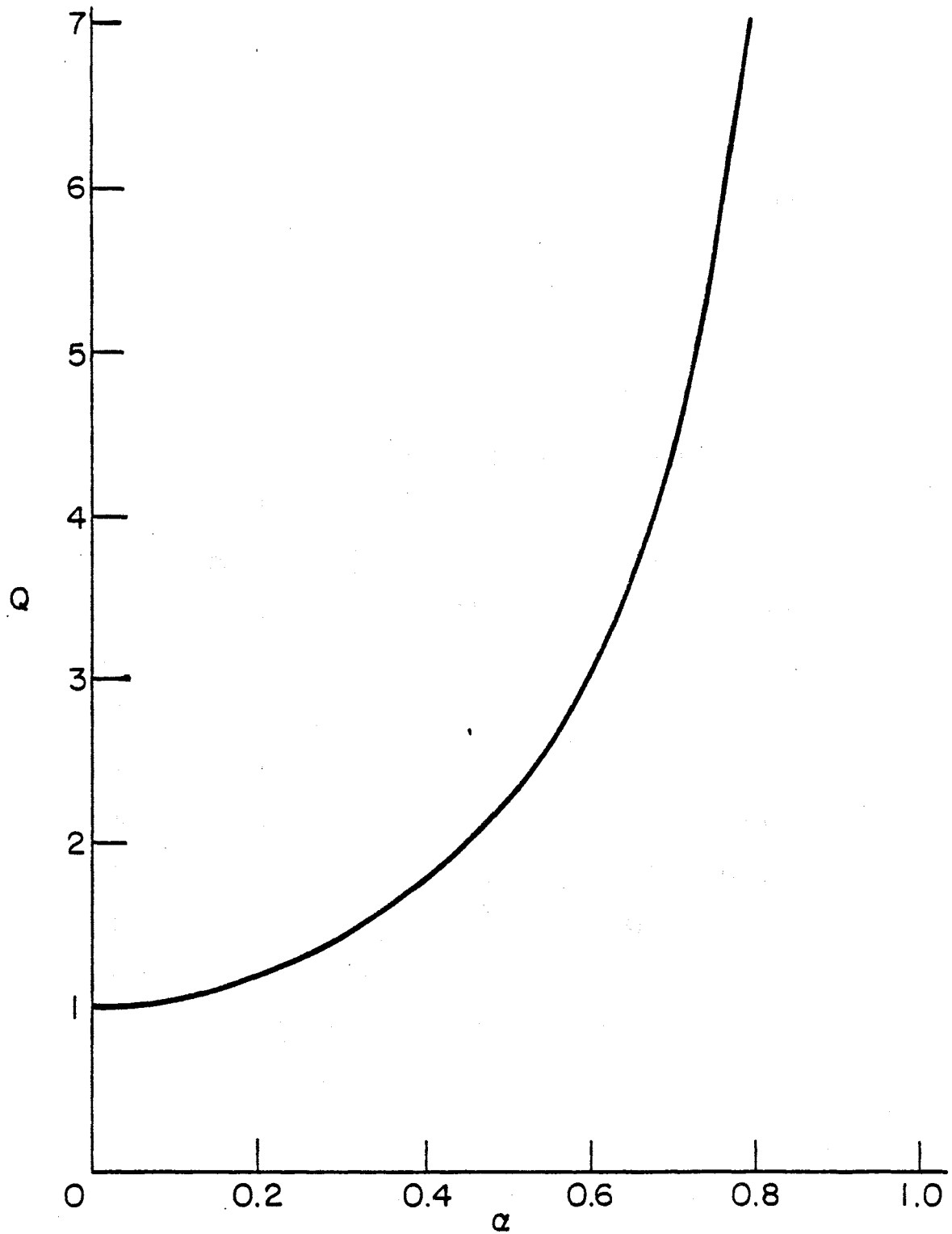


Fig. 15 Amplification of Back Free Surface Correction Factor
for Unrestricted Bending and Uniform Stress

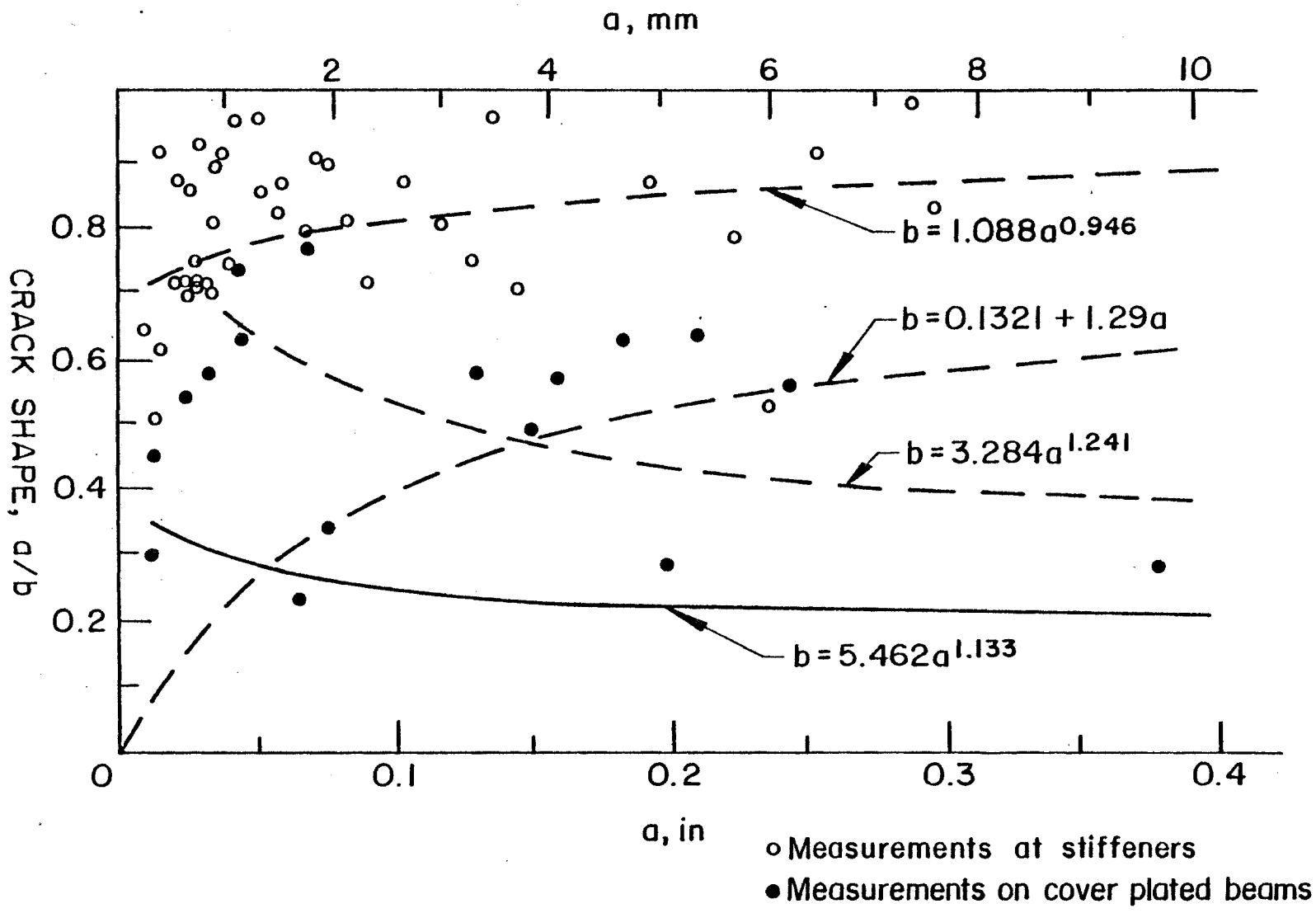


Fig. 16 Full Scale Beam Crack Shape

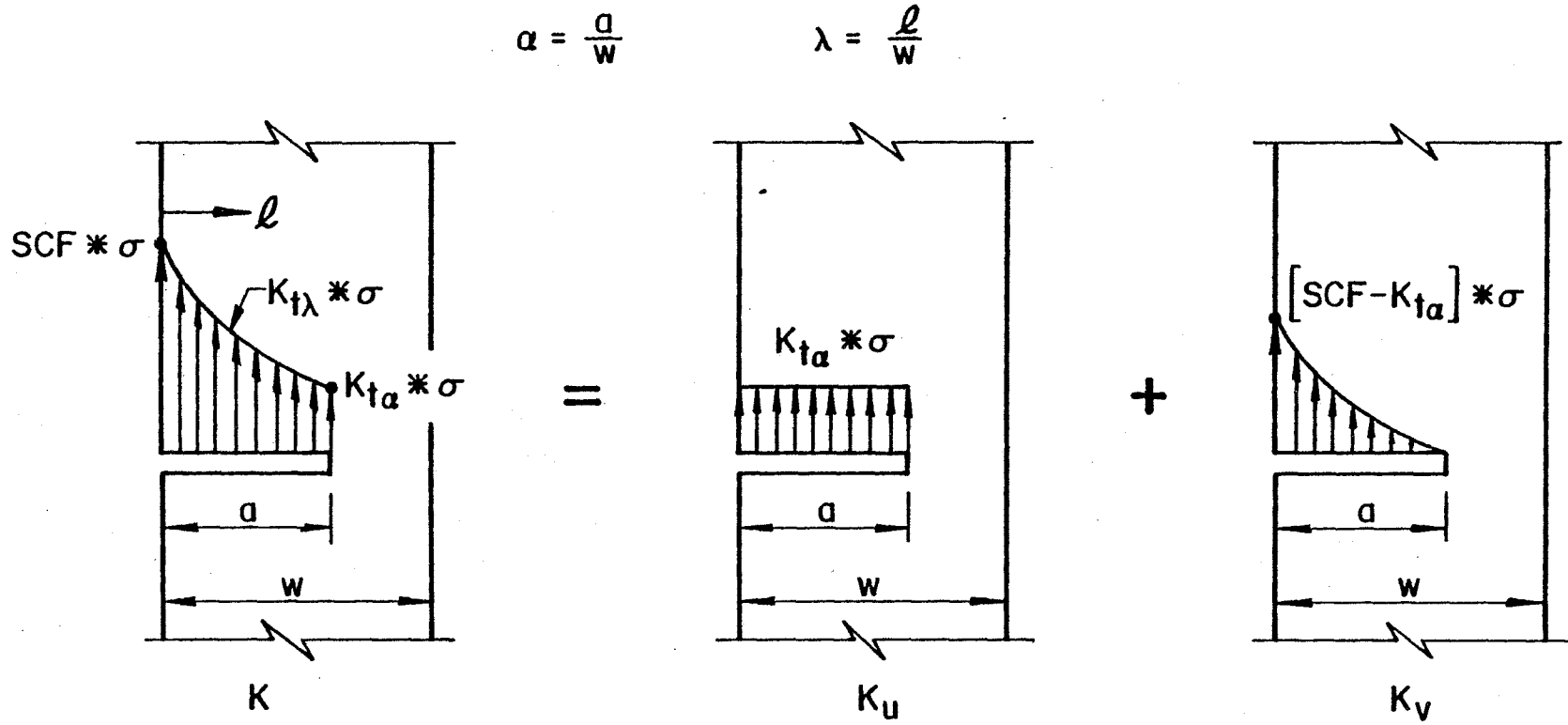
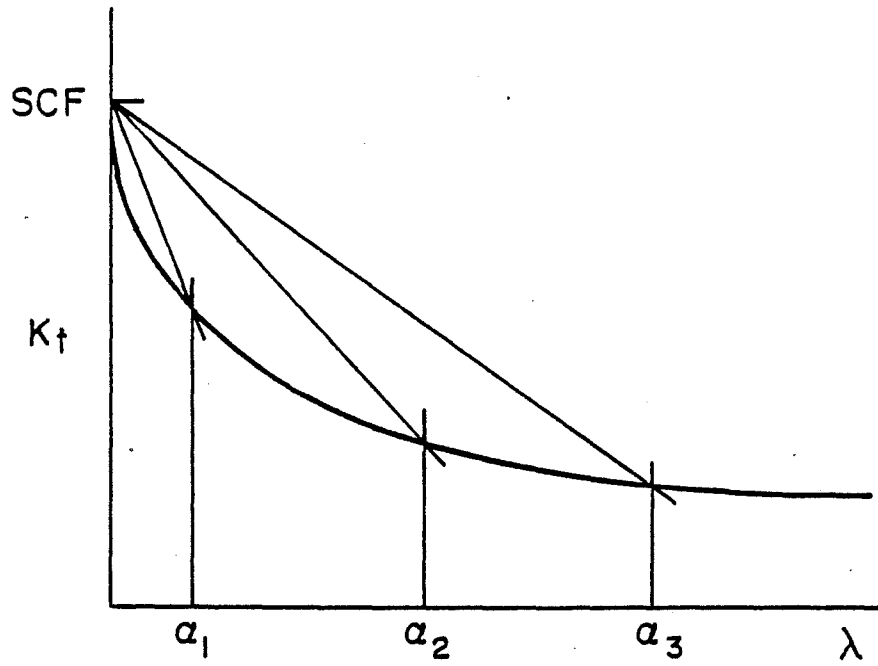
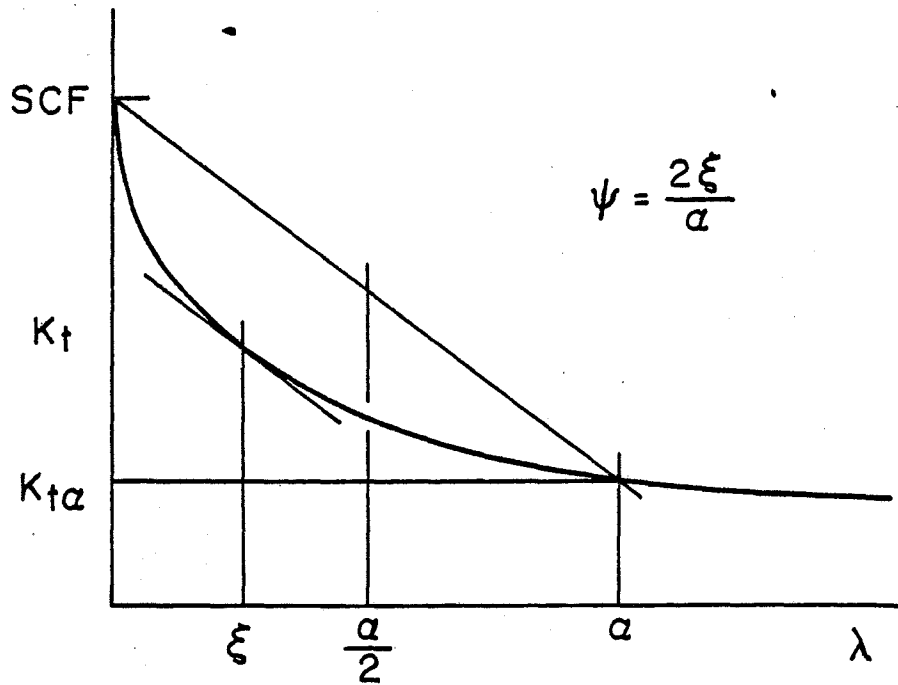


Fig. 17 Superposition of Stress Intensity Factors



(a) Proximity of variable stress subdistribution to linearity as a function of α



(b) ψ evaluation based on chord slope

Fig. 18 F_s Estimation for Variable Stress Subdistribution

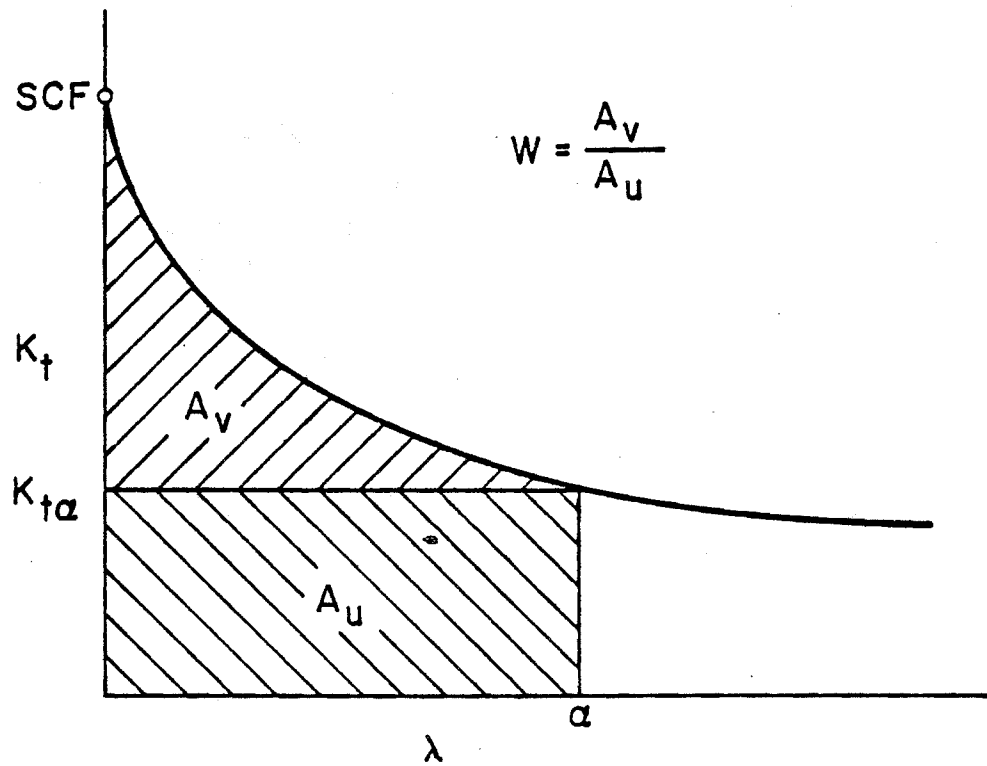


Fig. 19 Evaluation of Weighting Factor for Modifying
Through Crack Stress Gradient Correction Factor
Due to Crack Shape

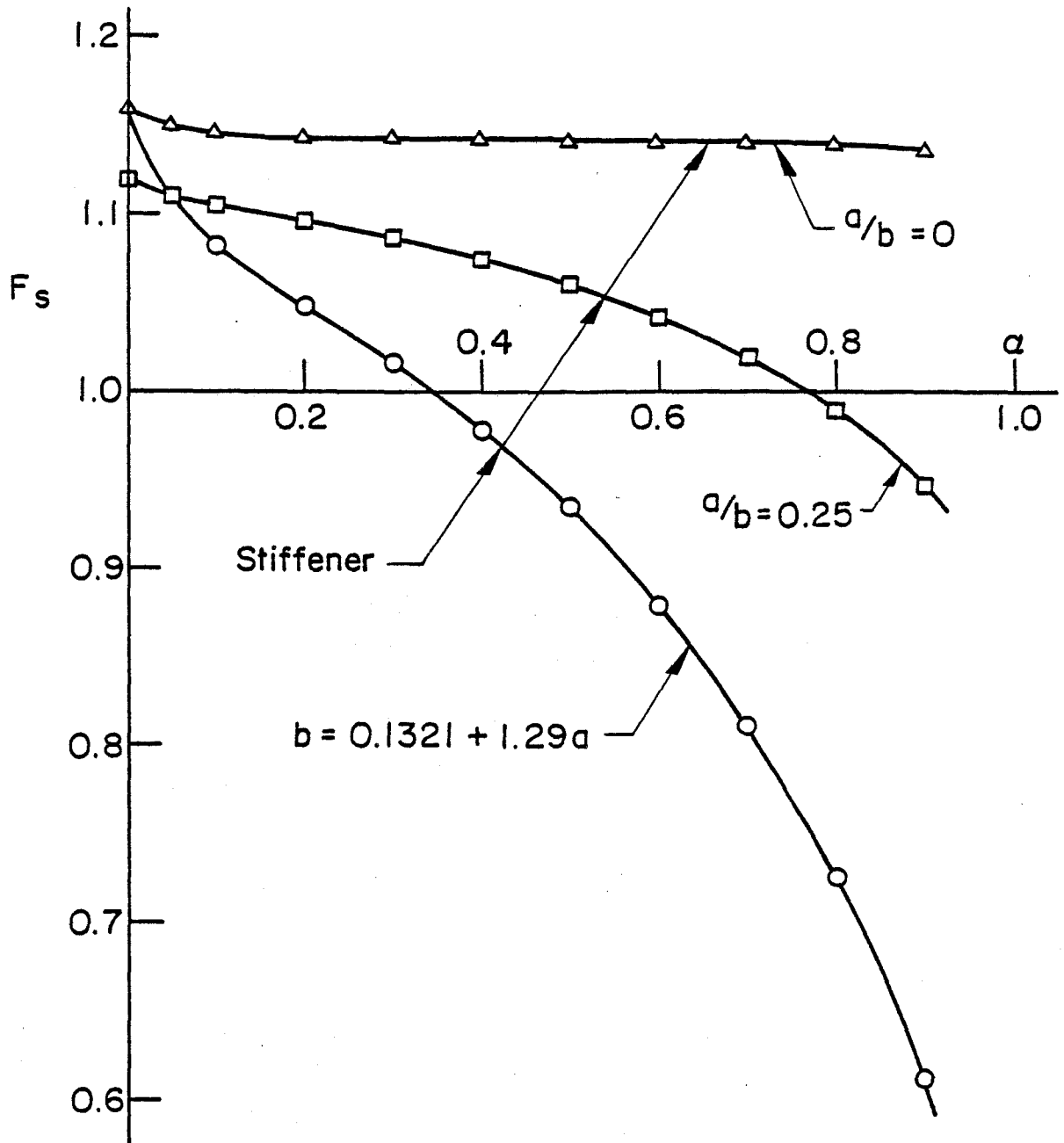


Fig. 20 Variation of Combined Front Free Surface Correction Factor at Stiffener Details

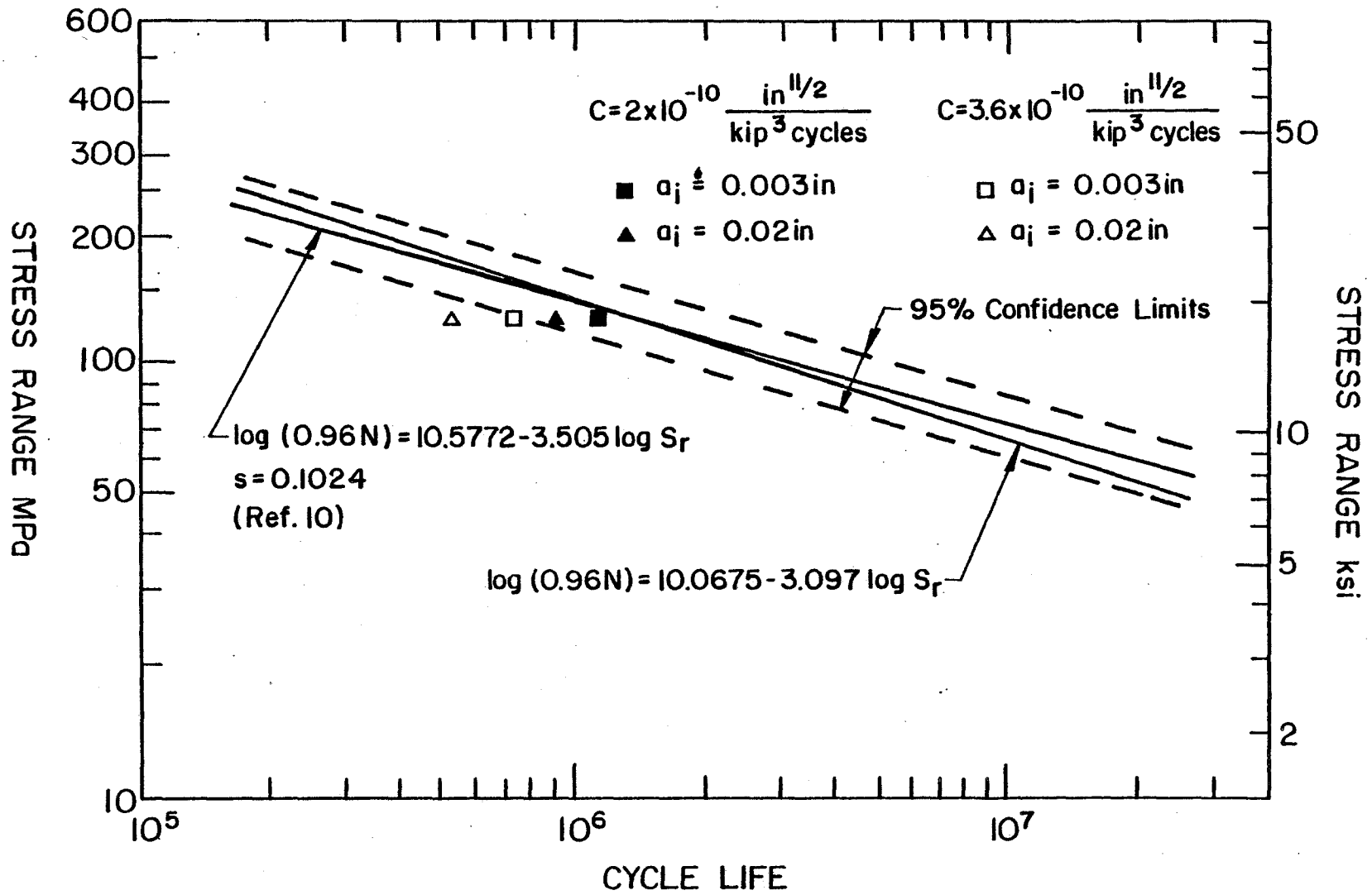


Fig. 21 Fatigue Life Estimates for Stiffeners Fillet-Welded to Flanges

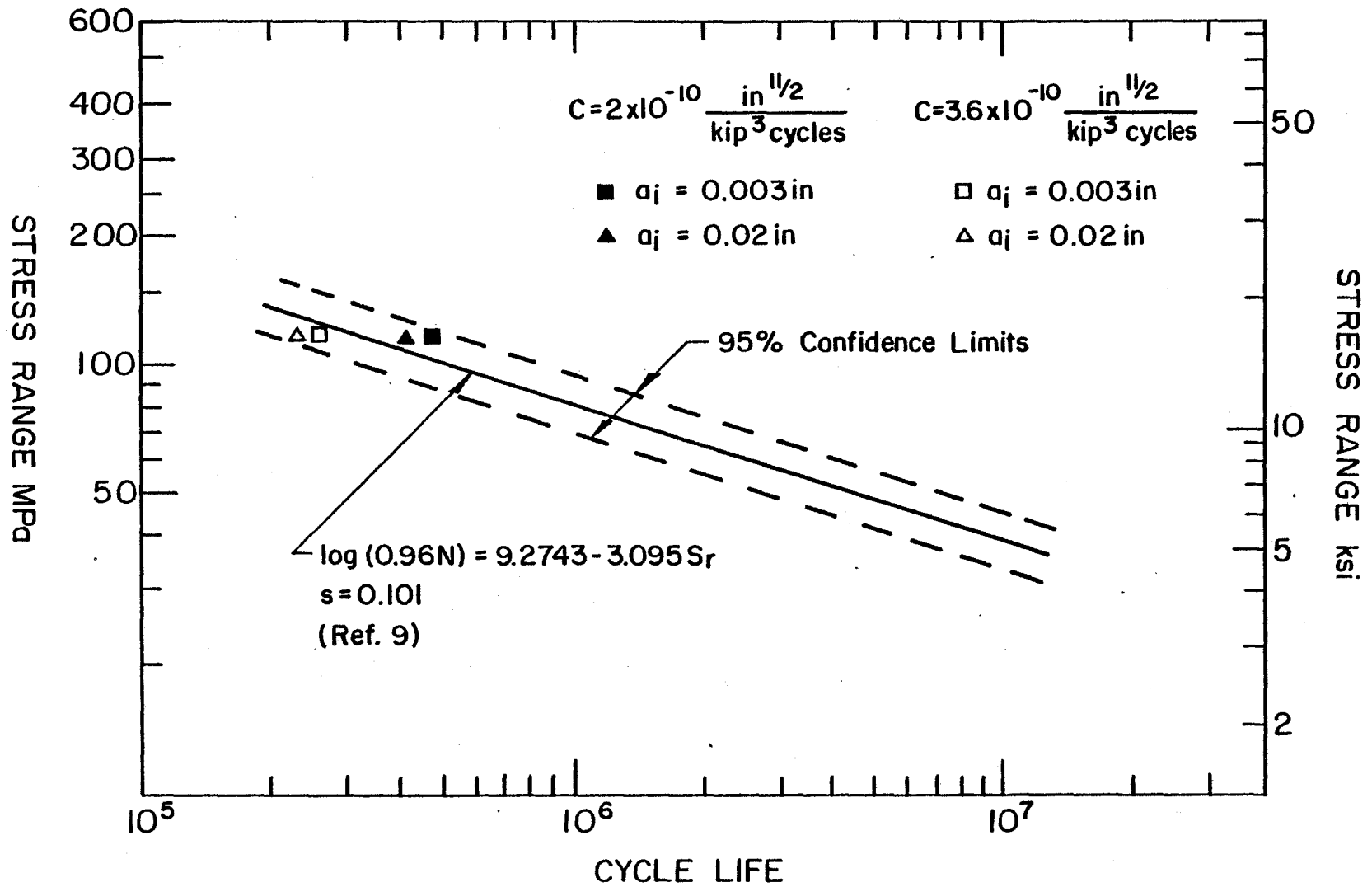


Fig. 22 Fatigue Life Estimates for Cover Plates with Transverse End Welds

8. NOMENCLATURE

- a = crack size; minor semidiameter of elliptical crack
- a_i = initial crack size
- a_f = final crack size
- A = number of cycles when stress range equals 1.0; stress concentration decay polynomial coefficient
- A_u = area of uniform stress subdistribution
- A_v = area of variable stress subdistribution
- b = major semidiameter of elliptical crack
- B = stress concentration decay polynomial coefficient
- c = stress concentration factor decay coefficient
- C = crack growth coefficient; stress concentration decay polynomial coefficient; coefficient for back surface correction secant radical to account for nonuniform stress distribution
- CF = combined total correction factor for stress intensity
- d = stress gradient correction factor decay coefficient
- D = stress concentration decay polynomial coefficient; constant in characteristic equation for ξ
- $E(k)$ = complete elliptic integral of the second kind
- F_e = crack shape correction factor
- F_g = stress gradient correction factor
- F'_g = stress gradient correction factor for circular crack
- \bar{F}_g = stress gradient correction factor for variable stress subdistribution applied to through crack

NOMENCLATURE

(continued)

- \bar{F}'_g = stress gradient correction factor for variable stress subdistribution applied to circular crack
- F_p = plastic zone correction factor
- F_s = front free surface correction factor
- F_{s1} = front free surface correction factor for a through crack with variable stress distribution
- F_{s2} = front free surface correction factor for a half-circular crack with variable stress distribution
- F_w = back free surface correction factor
- g = major semidiameter of elliptical hole in an infinite plate
- \mathcal{G} = strain energy release rate
- h = minor semidiameter of elliptical hole in an infinite plate
- k = $1 - (a/b)^2$
- K = stress intensity factor
- K_t = stress concentration factor
- $K_{t\alpha}$ = stress concentration factor at position α
- $K_{t\lambda}$ = stress concentration factor at position λ
- K_u = stress intensity factor for uniform stress subdistribution
- K_v = stress intensity factor for variable stress subdistribution
- ΔK = range of stress intensity factor
- ℓ = distance along crack path from origin
- \log = logarithm to base 10

NOMENCLATURE

(continued)

- L = attachment length
- m = number of finite elements to crack length a
- n = crack growth exponent; negative slope of log-log S_r -N curve
- N = fatigue life
- p = stress concentration factor decay exponent
- q = stress gradient correction factor decay exponent
- Q = amplification coefficient for F_w to account for bending
- s = standard error of estimate
- S_r = nominal stress range
- SCF = maximum stress concentration factor; stress concentration factor for the crack origin
- T_f = flange thickness
- T_{cp} = cover plate thickness
- w = plate dimension in direction of crack growth (T_f); crack length at which rate of growth becomes infinite
- W = ratio of area of variable stress subdistribution to area of uniform stress subdistribution, A_v/A_u
- W_f = flange width
- X = ratio of stress concentration factor at α to stress gradient correction factor for α
- Y = ratio of F'_g for circular crack to F_g for through crack for total stress distribution

NOMENCLATURE

(continued)

- Y' = ratio of F'_g for circular crack to F_g for through crack for variable stress subdistribution
- Y'' = ratio of F'_g for circular crack to F_g for through crack for uniform stress subdistribution
- Z = weld leg size
-
- α = nondimensionalized crack length, a/T_f or a/w
- γ = value of η associated with elliptical hole perimeter
- η = elliptic coordinate
- λ = nondimensionalized distance, ℓ/T_f or ℓ/w
- ξ = value of λ at which slope of decay curve equals slope of straight line from SCF to K_t at α
- σ = stress
- ϕ = angle from major semidiameter of elliptical crack
- ψ = measure of proximity of variable stress distribution to linearity; has value 1.0 if actually linear

9. REFERENCES

1. Albrecht, P. and Yamada, K.

RAPID CALCULATION OF STRESS INTENSITY FACTORS

J. Struct. Div., ASCE, Vol. 103, No. ST2, Proc. Paper
12742, pp. 377-389.

2. AASHTO Subcommittee on Bridges and Structures

INTERIM SPECIFICATIONS BRIDGES 1974

American Association of State Highway and Transportation
Officials, Washington, D.C., 1974.

3. AASHTO Subcommittee on Bridges and Structures

STANDARD SPECIFICATIONS FOR HIGHWAY BRIDGES

American Association of State Highway Officials, Washington,
D.C., 1973.

4. Bathe, K. J., Wilson, E. L., and Peterson, F. E.

SAP IV - A STRUCTURAL ANALYSIS PROGRAM FOR STATIC AND DYNAMIC
RESPONSE OF LINEAR SYSTEMS

Earthquake Engineering Research Center Report No. EERC,
73-11, U. of California, Berkeley, Ca., June 1973.

5. Biezeno, C. B. and Grammel, R.

ELASTIC PROBLEMS OF SINGLE MACHINE ELEMENTS

Vol. II, Engineering Dynamics, Blackie & Son, Ltd.,
London, England, 1956, pp. 84-90.

6. Bowie, O. L.

ANALYSIS OF AN INFINITE PLATE CONTAINING RADIAL CRACKS
ORIGINATING AT THE BOUNDARY OF AN INTERNAL CIRCULAR HOLE

J. Math. and Phys., Vol. 35, 1956, p. 60.

7. Roberts, R., Fisher, J. W., Irwin, G. R., Boyer, K. D.,
Hausammann, H., Krishna, G. V., Morf, U. and Slockbower, R. E.

DETERMINATION OF TOLERABLE FLAW SIZES IN FULL SIZE WELDED
BRIDGE DETAILS

Report No. FHWA-RD-77-170, Federal Highway Administration,
Office of Research and Development, Washington, D.C.,
December, 1977.

8. Bueckner, H. F.

THE PROPAGATION OF CRACKS AND THE ENERGY OF ELASTIC DEFORMATION

Trans., ASME, Vol. 80, 1958, p. 1225.

9. Fisher, J. W., Frank, K. H., Hirt, M. A., and McNamee, B. M.

EFFECT OF WELDMENTS ON THE FATIGUE STRENGTH OF STEEL BEAMS

NCHRP Report No. 102, Highway Research Board, National
Academy of Sciences - National Research Council,
Washington, D.C., 1970.

10. Fisher, J. W., Albrecht, P. A., Yen, B. T., Klingerman, D. J.,
and McNamee, B. M.

FATIGUE STRENGTH OF STEEL BEAMS WITH WELDED STIFFENERS
AND ATTACHMENTS

NCHRP Report No. 147, Transportation Research Board,
National Research Council, Washington, D.C., 1974.

11. Fisher, J. W.

BRIDGE FATIGUE GUIDE - DESIGN AND DETAILS

AISC, New York, N.Y., 1977.

12. Frank, K. H.

THE FATIGUE STRENGTH OF FILLET WELDED CONNECTIONS

Ph.D. Dissertation, Lehigh U., Bethlehem, Pa., October 1971.

13. Green, A. E. and Sneddon, I. N.

THE DISTRIBUTION OF STRESS IN THE NEIGHBORHOOD OF A FLAT
ELLIPTICAL CRACK IN AN ELASTIC SOLID

Proceedings, Cambridge Philosophical Society, Vol. 46, 1950,
p. 159.

14. Gurney, T. R.

FINITE ELEMENT ANALYSES OF SOME JOINTS WITH THE WELDS TRANSVERSE
TO THE DIRECTION OF STRESS

Welding Research International, Vol. 6, No. 4, 1976;

also, Welding Research Abroad, Vol. XXII, No. 10, December
1976.

15. Hayes, D. J. and Maddox, S. J.

THE STRESS INTENSITY FACTOR OF A CRACK AT THE TOE OF A FILLET
WELD

Welding Institute Research Bulletin, Vol. 13, No. 1,
January 1972.

16. Hayes, D. J.

A PRACTICAL APPLICATION OF BUECKNER'S FORMULATION FOR DETER-
MINING STRESS INTENSITY FACTORS FOR CRACKED BODIES

International J. Fracture Mech., Vol. 8, No. 2, June
1972, p. 157.

17. Hirt, M. A. and Fisher, J. W.

FATIGUE CRACK GROWTH IN WELDED BEAMS

Eng. Frac. Mech., Vol. 5, 1973, p. 415.

18. Irwin, G. R. and Kies, J. A.

CRITICAL ENERGY RATE ANALYSIS OF FRACTURE STRENGTH

Welding J., Vol. 33, No. 4, April 1954, p. 193-s.

19. Irwin, G. R.
ANALYSIS OF STRESSES AND STRAINS NEAR THE END OF A CRACK
TRAVERSING A PLATE
Trans., ASME, Series E, Vol. 79, September 1957, p. 361.
20. Irwin, G. R.
FRACTURE
Handbuch der Physik, Vol. VI, Springer, Berlin, Germany,
1958, p. 551.
21. Kobayashi, A. S.
A SIMPLE PROCEDURE FOR ESTIMATING STRESS INTENSITY FACTOR IN
REGION OF HIGH STRESS GRADIENT
Significance of Defects in Welded Structures, Proc., 1973
Japan-U.S. Seminar, U. of Tokyo Press, Tokyo, Japan,
1974, p. 127.
22. Maddox, S. J.
ASSESSING THE SIGNIFICANCE OF FLAWS IN WELDS SUBJECT TO FATIGUE
Welding Journal, Vol. 53, No. 9, September 1974, p. 401-s.
23. Maddox, S. J.
AN ANALYSIS OF FATIGUE CRACKS IN FILLET WELDED JOINTS
International J. Fracture Mech., Vol. 11, No. 2, April
1975, p. 221.

24. Neal, D. M.

STRESS INTENSITY FACTORS FOR CRACK EMANATING FROM RECTANGULAR
CUTOUTS

International J. Fracture Mech., Vol. 6, No. 4, December
1970, p. 393.

25. Neuber, H.

KERBSPANNUNGSLEHRE

2nd ed., Springer-Verlag, Berlin, Germany, 1958, pp. 52-
56.

26. Newman, J. C., Jr.

AN IMPROVED METHOD OF COLLOCATION FOR THE STRESS ANALYSIS OF
CRACKED PLATES WITH VARIOUS SHAPED BOUNDARIES

NASA TN D-6376, NASA Langley Research Center, Hampton,
Va., August, 1971.

27. Paris, P. C., Gomez, M. P. and Anderson, W. E.

A RATIONAL ANALYTICAL THEORY OF FATIGUE

The Trend in Engineering, U. of Washington, Seattle, Wa.,
Vol. 13, No. 1, January 1961.

28. Paris, P. C. and Sih, G. C.

STRESS ANALYSIS OF CRACKS

Fracture Toughness Testing and Its Applications, STP 381,
ASTM, Phila., Pa., 1965, p. 30.

29. Randall, P. N.

SEVERITY OF NATURAL FLAWS AS FRACTURE ORIGINS, AND A STUDY OF
THE SURFACE-CRACKED SPECIMEN

AFML-TR-66-204, August 1966 (published in ASTM STP 410,
p. 88).

30. Rice, J. R.

MECHANICS OF CRACK TIP DEFORMATION AND EXTENSION BY FATIGUE

Fatigue Crack Propagation, STP 415, ASTM, Phila., Pa.,
1966, p. 247.

31. Signes, E. G., Baker, R. G., Harrison, J. D., and Burdekin, F. M.

FACTORS AFFECTING THE FATIGUE STRENGTH OF WELDED HIGH STRENGTH
STEELS

British Welding Journal, Vol. 14, No. 3, March 1967,
p. 108.

32. Sih, G. C.

HANDBOOK OF STRESS INTENSITY FACTORS

Inst. of Frac. and Solid Mech., Lehigh U., Bethlehem,
Pa., 1973.

33. Sommer, E., Hodulak, L., and Kordisch, H.

GROWTH CHARACTERISTICS OF PART-THROUGH CRACKS IN THICK-WALLED
PLATES AND TUBES

(to be published in ASME Trans.).

34. Tada, H., Paris, P. C., and Irwin, G. R.
THE STRESS ANALYSIS OF CRACKS HANDBOOK
Del Research Corporation, Hellertown, Pa., 1973.
35. Tada, H. and Irwin, G. R.
K-VALUE ANALYSIS FOR CRACKS IN BRIDGE STRUCTURES
Fritz Eng. Lab. Report No. 399.1, Lehigh U., Bethlehem,
Pa., June 1975.
36. Watkinson, F., Bodger, P. H., and Harrison, J. D.
THE FATIGUE STRENGTH OF WELDED JOINTS IN HIGH STRENGTH STEELS
AND METHODS FOR ITS IMPROVEMENT
Proc., Fatigue of Welded Structures Conf., Welding
Institute, Brighton, England, 1971.
37. Zettlemyer, N.
STRESS CONCENTRATION AND FATIGUE OF WELDED DETAILS
Ph.D. Dissertation, Lehigh U., Bethlehem, Pa., October
1976.
38. Zettlemyer, N. and Fisher, J. W.
STRESS GRADIENT CORRECTION FACTOR FOR STRESS INTENSITY AT
WELDED STIFFENERS AND COVER PLATES
Welding Journal, Vol. 56(12), December 1978, Research
Supplement, pp. 393s-398s.

39. Slockbower, R. E. and Fisher, J. W.

FATIGUE RESISTANCE OF FULL SCALE COVER-PLATED BEAMS

Fritz Engineering Laboratory, Report 386-9(78), June 1978.

10. ACKNOWLEDGMENTS

This investigation was part of PennDOT Research Project No. 72-3, a study of high cycle fatigue of welded details, sponsored by the Pennsylvania Department of Transportation and the Federal Highway Administration.

The analytical study reported herein was conducted at the Fritz Engineering Laboratory, Lehigh University, Bethlehem, Pennsylvania. The authors wish to acknowledge the help of Dr. George R. Irwin and Hans Hausammann for valuable discussions and assistance.

Appreciation is also due Mrs. Ruth Grimes who typed the manuscript and Mr. John Gera and Mrs. Sharon Balogh for preparation of the figures.